Graphitic carbon nitride "reloaded": emerging applications beyond (photo)catalysis

Jian Liu,*[ab] Hongqiang Wang*[cd] and Markus Antonietti[a]

Despite being one of the oldest materials described in the chemical literature, graphitic carbon nitride (g-C_3N_4) has just recently experienced a renaissance as a highly active photocatalyst, and the metal-free polymer was shown to be able to generate hydrogen under visible light. The semiconductor nature of g-C_3N_4 has triggered tremendous endeavors on its structural manipulation for enhanced photo(electro)chemical performance, aiming at an affordable clean energy future. While pursuing the stem of g-C_3N_4 related catalysis (photocatalysis, electrocatalysis and photoelectrocatalysis), a number of emerging intrinsic properties of g-C_3N_4 are certainly interesting, but less well covered, and we believe that these novel applications outside of conventional catalysis can be favorably exploited as well. Thanks to the general efforts devoted to the exploration and enrichment of g-C_3N_4 based chemistry, the boundaries of this area have been possibly pushed far beyond what people could imagine in the beginning. This review strives to cover the achievements of g-C_3N_4 related materials in these unconventional application fields for depicting the broader future of these metal-free and fully stable semiconductors. This review starts with the general protocols to engineer g-C_3N_4 micro/nanostructures for practical use, and then discusses the newly disclosed applications in sensing, bioimaging, novel solar energy exploitation including photocatalytic coenzyme regeneration, templating, and carbon nitride based devices. Finally, we attempt an outlook on possible further developments in g-C_3N_4 based research.

1. Introduction

Carbon nitride oligomers and polymers have a pretty long history. The first example in the carbon nitride family could be traced back to the 1830s, when Berzelius and Liebig, respectively, reported the general formula $(C_3N_3H)_n$ and coined the notation "melon".[1,2] Since 1989, work has been inspired by Liu and Cohen's theoretical prediction that the β-polymorph of hydrogen-free C_3N_4 would be a super hard material.[3] Meanwhile, graphitic carbon nitride (g-C_3N_4) has attracted much attention, as it is the most stable allotrope. Being structurally similar to graphite, g-C_3N_4 bears strong covalent C–N bonds instead of C–C bonds in each layer, while the layers are bound by van der Waals forces, only. The framework topology identified in most "real-world" g-C_3N_4-substances is a defect-rich, N-bridged "poly(tri-s-triazine)".

[a] Department of Colloid Chemistry, Max Planck Institute of Colloids and Interfaces, 14424 Potsdam, Germany

[b] Department of Chemistry, Northwestern University, Evanston, Illinois 60208, USA. E-mail: Jianliu@northwestern.edu

[c] Center for Nano Energy Materials, State Key Laboratory of Solidification Processing, School of Materials Science and Engineering, Northwestern Polytechnical University, Xi'an, 710072, P. R. China

[d] Department of Chemistry, Stephenson Institute for Renewable Energy, University of Liverpool, Peach Street, Liverpool, L69 7ZF, UK. E-mail: hongqiang.wang@nwpu.edu.cn

The tri-s-triazine ring structure and the high degree of condensation provide the polymer with high stability with respect to thermal (up to 600 °C in air) and chemical attack (for example, acid, base, and organic solvents), and an appealing electronic structure, i.e. being a medium-bandgap, indirect semiconductor. These features principally already allow its direct use in sustainable chemistry as a multifunctional heterogeneous metal-free catalyst.

However, g-C_3N_4 was not used as a metal-free heterogeneous catalyst until 2006 when a mesoporous version was used for catalyzing Friedel–Crafts reaction.[4] The subsequent discovery of visible-light-driven photocatalytic activity of g-C_3N_4 for hydrogen evolution by the same group in 2009 disclosed g-C_3N_4 as a new generation of metal-free polymeric photocatalysts.[5] Since then, the number of studies on the catalytic, electrocatalytic, and photocatalytic performance of graphitic carbon nitride has been steadily increasing.[4,5] Future energy and environmental issues by developing facile and economic visible-light-driven photocatalysts for environment remediation and energy conversion have been addressed, such as photocatalytic H_2 evolution from water, photodegradation of organic pollutants, photoelectric conversion, CO_2 activation, and other important catalytic reactions. Selecting "graphitic carbon nitride" as a topic in the search engine of Web of Science, over 1900 publications could be found, indicating the enormous interest in g-C_3N_4. Meanwhile and by all these joint efforts, a bunch of breakthrough studies have

appeared on the stage, for instance, the quantum efficiency of g-C$_3$N$_4$ based photocatalytic hydrogen evolution with a sacrificial agent now exceeds 7%;[6,7] the graphitic carbon nitride based composite (with polypyrrole and carbon quantum dots, respectively) revealed the potential for accomplishing overall water splitting.[8] An electrocatalyst composed of graphenes and carbon nitrides, only, can potentially replace platinum catalysts in electrochemical hydrogen evolution.[9–11] The future practical application of g-C$_3$N$_4$ for sustainable chemistry is thus coming closer and becoming visible.

The rediscovery of g-C$_3$N$_4$ spurred the interest in other versatile applications also. This can be exemplified by intensive interest in the investigation of its sensing properties.[12] Usually, structuring of g-C$_3$N$_4$ into controlled morphologies, especially its shaped nanosheets, substantially helps the enhancement of response and consequently the sensitivity, leading to the rapid development of nanosheet based sensors with a superior detection limit for different targets.[13,14] Coupling with other substances (graphene, semiconductors, metals, etc.) could boost the sensing capabilities, and importantly, bring out a new sensing mechanism. While structuring plays important roles in the development of g-C$_3$N$_4$ based sensing, progress in discovering the novel intrinsic properties of g-C$_3$N$_4$, such as its suitability for two-photon absorbance,[15] is becoming a key to understand this material in a broader context. For instance, an alternative for traditional fluorescence sensing has been developed based on a new electrochemical phenomenon of g-C$_3$N$_4$, i.e. electrogenerated chemiluminescence.[16] The facile structural manipulation and amazing phenomena recently discovered have extended g-C$_3$N$_4$ based research from sensing to bioimaging, solar cells, nanoarchitecture processes, and nonvolatile memory devices.[17–20]

The advantageous features of g-C$_3$N$_4$ (simple composition, facile synthesis, low cost, and rich chemistry) have therefore stimulated researchers in a broader range, however inspiring reviews so far have mainly focused on graphitic carbon nitride for (photo)catalysis.[21–23] In the present review article, we intend to close this gap and target a relatively comprehensive and updated review on its emerging applications beyond catalysis. As many of these novel applications and modifications come with inherent features also useful for photocatalysis, we expect that with the new properties of g-C$_3$N$_4$ being continually discovered, scientists with different research backgrounds will inspire each other, thus enabling faster, further progress of carbon nitride and other related research studies.

2. g-C$_3$N$_4$ family with diverse micro-/nanostructures

The intense recent studies led to the generation of a g-C$_3$N$_4$ family with abundant micro-/nanostructures and morphologies, which are still being extended every day. Synthetic routes,

Jian Liu received his PhD degree in Physical Chemistry with Prof. Yanlin Song from Institute of Chemistry, Chinese Academy of Sciences in 2011. In January of 2012, he joined Prof. Markus Antonietti's group at the Max-Planck Institute of Colloids and Interfaces with an Alexander von Humboldt Research Postdoctoral Fellowship. After two and half years stay in the Department of Colloid Chemistry, he moved to Prof. Mercouri G. Kanatzidis's group at Northwestern University (Evanston, US) for further studying. His current scientific interest is mainly focused on the synthesis of bio-inspired functional materials for solar energy and environmental science.

Jian Liu

Hongqiang Wang received his PhD in Condensed Matter Physics at the Institute of Solid State Physics, Chinese Academy of Sciences, in 2008. He then worked, respectively, as a Postdoctoral Researcher, an Alexander von Humboldt Fellow and a Marie Curie Intra-European Fellow in National Institute of Advanced Industrial Science and Technology (Japan), Max Planck Institute of Colloids and Interfaces (Germany), and University of Liverpool (UK). He has been a Professor in Northwestern Polytechnical University (China) since 2015. His main research interest is the extremely non-equilibrium processing and its use for generating novel functional materials.

Hongqiang Wang

Markus Antonietti is a Director of the Max Planck Institute of Colloids and Interfaces and has recently focused on sustainable materials for the energy change. He has written about 650 original papers and is well cited in the field of functional polymers, porous materials, heterogeneous organocatalysis, and artificial photosynthesis.

Markus Antonietti

This journal is © The Royal Society of Chemistry 2016

Chem. Soc. Rev., 2016, **45**, 2308–2326 | 2309

condensation temperatures, and the material compositions and morphologies are important factors to determine the attained structure and morphology, which strongly relate to its properties and applications of g-C_3N_4. Furthermore, vivid structural manipulation has always been driven by specific functionality/performance expectations, which gives rise to particular micro/nanoarchitectures, such as mesoporous structures, nanosheets, nanorods, hierarchical structures and films. In order to give reader a clearer picture of the available morphologies also for non-conventional applications, an overview over synthesized nanostructures is given. Though being challenging, we classify herein in terms of the decrease of dimensions, as shown in Fig. 1.

2.1   Bulky g-C_3N_4

Bulk g-C_3N_4 usually served as the benchmark material for comparison. Bulky g-C_3N_4 can be simply obtained by the thermal condensation of a variety of nitrogen-rich precursors without direct C–C bonding, such as cyanamide, dicyandiamide, melamine, thiourea, urea, or mixtures. However, such kinds of bulky carbon nitride materials obtained by this route are bulk materials which possess a very low surface area, normally below 10 m^2 g^{-1}. Not long ago, Jun and Shalom independently developed a method to synthesize g-C_3N_4 with a relatively high surface area by utilizing the pre-organized supramolecular complex of melamine and cyanuric acid, thus allowing the direct access of rather small crystals by topotactic transformations.[24,25] It is to be mentioned that in typical bulk processes, the specific surface area of such topotactical template structures can reach 60–80 m^2 g^{-1}.

Fig. 1   Rich morphologies of the g-C_3N_4 family with dimensions ranging from bulk to quantum dots. (Reprinted with permission from Macmillan Publishers Ltd: [*Nat. Commun.*] (ref. 7), copyright (2012). Adapted with permission from ref. 11. Copyright (2012) the Wiley-VCH. Adapted with permission from ref. 17. Copyright (2012) American Chemical Society. Adapted with permission from ref. 33. Copyright (2012) the Wiley-VCH. Adapted with permission from ref. 37. Copyright (2012) American Chemical Society. Reproduced from ref. 46 with permission from the Royal Society of Chemistry. Ref. 39 – Published by the Royal Society of Chemistry.)

2.2   Mesoporous g-C_3N_4

Porosity control is becoming important for the diversified applications of g-C_3N_4. Mesoporous g-C_3N_4 (abbreviated as mpg-C_3N_4) can be obtained by nanocasting/replication of silica spheres or mesoporous silica objects, a process well established for mesostructured materials.[26] In a typical synthesis, commercially available silica sol and cyanamide are mixed in aqueous solutions. After the complete removal of water in an oil bath, the resulting composite is transferred to a crucible with a lid and heated for 4 h at 550 °C to condense the precursor into polymeric carbon nitride. After dissolving the silica template by ammonia hydrogen difluoride, mpg-C_3N_4 could be obtained with surface areas of up to 350 m^2 g^{-1}. g-C_3N_4 monoliths inheriting the structure from a templated precursor while featuring porous inner structure were also reported.[6] Uniformly distributed carbon nitride particles with mesopores could be also obtained by etched/synthesized silica sphere templating.[7,27,28]

2.3   g-C_3N_4 nanosheets and thin films

Inspired by the huge success of graphene exfoliated from bulk graphite, the rational extension of the graphene strategy to layered g-C_3N_4 is possible. This is based on the fact that the structure is set-up by a graphite-like layered structure with strong C–N covalent bonding in-plane and weak van der Waals interaction across the layers. Zhang *et al.* reported a sonication-assisted liquid-exfoliation top-down method to prepare thin-layer g-C_3N_4 nanosheets from bulk g-C_3N_4.[17,29,30] It is known that the layered materials can be successfully exfoliated in solvent media with surface energy matching with the materials. Zhang *et al.* also calculated the surface energy of g-C_3N_4 as 115 mJ m^{-2}, higher than that of water ($\sim$72 mJ m^{-2}). Compared with graphene with a surface energy of around 45 mJ m^{-2}, carbon nitride nanosheets are therefore very polar/polarizable and attract each other, but also other substances perpendicular to the planes about 3 times as strong as graphenes. Due to the strong repulsion from surface charges among nanosheets, dispersions of ultrathin g-C_3N_4 nanosheets are however usually very stable, sometimes without precipitating upon standing for more than several months. There are also other protocols reported for acquiring such two dimensional structures. Niu *et al.* developed a facile thermal-oxidation route to exfoliate the dicyandiamide-derived bulky g-C_3N_4 into nanosheets with a high surface area of 300 m^2 g^{-1}.[31] Crystalline carbon nitride nanosheets were reported by the exfoliation of as-obtained poly(triazine imide) synthesized by the ionothermal synthesis.[32,33]

As an ideally infinite extension of a nanosheet in two dimensions, thin films of g-C_3N_4 are crucial for the development of flat devices. The first conductive layers for electrode applications were reported by Shalom *et al.*, however still afflicted with grain boundaries and interstitial voids.[10] Liu *et al.* developed a nanoconfinement method to fabricate graphitic carbon nitride films directly on conductive substrates.[34] An "ink" (cyanamide aqueous solution) infiltrated anodic aluminum oxide (AAO) stamp is found to be capable of "ink-jetting" carbon nitride films featuring regular microstructures of the stamp onto the substrates
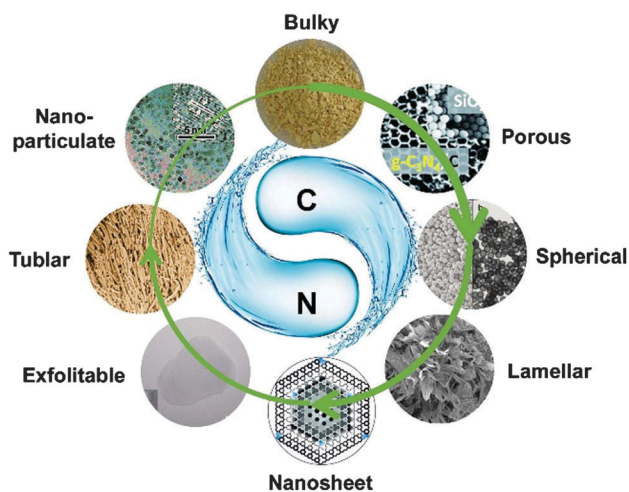
2310 | *Chem. Soc. Rev.*, 2016, 45, 2308–2326

This journal is © The Royal Society of Chemistry 2016

via in situ "chemical vapor deposition" (CVD). Bian *et al.* simplified the synthesis by putting a substrate covering the crucible mouth and the g-C$_3$N$_4$ film could also obtained after the "CVD" process. However, the absence of the AAO template led to a lack of control over the film morphology.[35] To endow carbon nitride films with more functionalities, Jia and coworkers developed a hierarchical macro-/mesoporous carbon nitride film on any desired substrate by employing dual templates, and the film was found to be useful in sensing applications.[36]

2.4 One dimensional g-C$_3$N$_4$ nanowires/nanorods/nanotubes

By virtue of smooth carrier transport, nanostructured g-C$_3$N$_4$ in its one dimensional forms could promise the potential electrical/optoelectric properties and photocatalytic applications as well. Taking advantage of the porous channel of AAO, Li *et al.* reported the fabrication of g-C$_3$N$_4$ nanorods, however, inter-rod hexagonal packing of the template was not successfully transferred in the final sample.[37] Liu *et al.* found that using suitable diatom frustules with smaller size as templates, cyanamide could be condensed inside the diatom frustule channels, and thereby hierarchical carbon nitride arrays could be obtained after removing the diatom template.[38] While nanorod structures are very common for g-C$_3$N$_4$ synthesis, the larger length-aspect ratio counterpart, g-C$_3$N$_4$ nanowires, is relatively rare to find in the literature. Liu *et al.* reported a special diatom frustule mediated direct growth of g-C$_3$N$_4$ nanowires from the underlying substrate.[39] Zhao *et al.* reported the large scale synthesis of nitrogen-rich carbon nitride microfibers by thermal evaporation of as-synthesized graphitic carbon nitride.[40]

Guo *et al.* reported the direct synthesis of carbon nitride nanotubes with inner diameters of 50–100 nm and wall thicknesses of 20–50 nm with the correct C$_3$N$_4$ stoichiometry. The high yield synthesis was accomplished *via* a simple benzene-thermal process involving the reaction of C$_3$N$_3$Cl$_3$ with NaN$_3$ in a Teflon-lined autoclave at 220 °C without using any catalyst or template.[41] Li *et al.* adopted a high pressure route at elevated temperature, and they synthesized carbon nitride nanobelts and nanotubes through the polycondensation of dicyandiamide (H$_4$C$_2$N$_4$) and melamine (C$_3$N$_6$H$_6$) at 290 °C and 4.5–5 MPa.[42] Bian *et al.* reported the synthesis of carbon nitride nanotubes by using porous anodic aluminum oxide membranes as templates through a polymerization reaction between ethylenediamine and carbon tetrachloride, with the final material acting as a catalyst support for cyclohexene dehydrogenation.[43] However, the carbon-to-nitrogen ratio of the material was 4.9 (significantly higher than the theoretical value of 0.75) and is thereby presumably better described as an N-doped carbon.

2.5 g-C$_3$N$_4$ zero dimensional quantum dots (QDs)

As a metal-free polymeric material, g-C$_3$N$_4$ QDs have the advantages of bright fluorescence, good stability, water-solubility, biocompatibility, and nontoxicity, making them good candidates in place of traditional QDs. In 2005, Groenewolt *et al.* synthesized carbon nitride QDs in mesoporous silica host matrices by sacrificial templating, and the 5 nm sized QD showed blueshifted photoluminescence compared with the bulky counterpart.[26] Highly blue

fluorescent graphitic carbon nitride QDs were synthesized using a simple microwave mediated method from formamide by Barman *et al.*[44] Zhang *et al.* developed fairly simple and green hydrothermal treatment of bulk g-C$_3$N$_4$ to form fluorescent g-C$_3$N$_4$ dots with blue emission, while Zhou *et al.* adopted a solid phase method to obtain such fluorescent dots.[45,46]

2.6 g-C$_3$N$_4$ composites

A large number of substances have been coupled with g-C$_3$N$_4$ to form compositions, including metal oxides (*e.g.*, TiO$_2$, ZnO, WO$_3$, Cu$_2$O, In$_2$O$_3$, Fe$_2$O$_3$, CdS, BiVO$_4$, graphene, carbon quantum dots and polypyrrole). Two types of synthetic methods are mainly employed for the synthesis of g-C$_3$N$_4$ based composites. The first one is mixing the substance with a carbon nitride precursor followed by the thermal condensation at desired temperature; the second one is the post-treatment of the substance with as-formed g-C$_3$N$_4$ by deposition or simply mixing. By combining with a diatom frustule template using the "incipient wetness impregnation" method, Liu *et al.* could deposit g-C$_3$N$_4$ coating onto the frustule and therefore an artificial "photosynthetic membrane" was built.[47]

3. Intrinsic features/properties of graphitic carbon nitride

3.1 Being metal free

Its merit of being metal free has always been linked with graphitic carbon nitride from the very beginning. The constitution elements for g-C$_3$N$_4$ are just C, N, and usually residual hydrogen in defects and for surface termination. It is noteworthy that the fabrication of an ideal graphitic carbon nitride with a C/N stoichiometric ratio of 0.75 is very difficult. Elemental analysis could provide evidence for incomplete condensation and the coupled excess of nitrogen. An average C/N atomic ratio of 0.72 is usually obtained (comparing with the theoretical 0.75), as well as trace but not ignorable amounts of hydrogen (2%) from uncondensed amino functions. The simple constitution of g-C$_3$N$_4$ renders the materials nontoxic and biocompatible for some biological applications. Zhang *et al.* investigated the biocompatibility and nontoxicity of g-C$_3$N$_4$ by incubating the HeLa cells with g-C$_3$N$_4$ materials.[17] It turned out that the HeLa cells could maintain activity after incubation with g-C$_3$N$_4$ nanosheets with concentrations of up to 600 μg mL^{-1} in aqueous solution.

3.2 Optical properties

Optical properties including diffuse reflectance spectroscopy and photoluminescence are important for various applications. The optical properties of graphitic carbon nitride are usually characterized by UV/Vis diffuse reflectance spectroscopy and photoluminescence. As illustrated in the diffuse reflectance spectrum, graphitic carbon nitride shows the typical absorption pattern of an organic semiconductor with a bandgap onset adsorption at about 420 nm. Graphitic carbon nitride usually exhibits strong blue photoluminescence at room temperature. The luminescence is observed over a wide range (430–550 nm)

and has a maximum at about 470 nm. Zhang *et al.* demonstrated the luminescence of g-C_3N_4 to be dependent on condensation temperature.[48] Electrically generated chemiluminescence of g-C_3N_4 was also discovered.[16,49]

g-C_3N_4 was also shown to possess a favorable two-photon absorbance behavior.[15] g-C_3N_4 could simultaneously absorb two near-infrared photons and emit bright fluorescence in the visible light region. Zhang *et al.* showed that when excited by the 780 nm red laser, g-C_3N_4 emitted strong green light.[15] However, there is a large red shift of the emission spectrum of g-C_3N_4 through two-photon excitation with respect to one-photon excitation, while for other semiconductors, the emission spectra of two-photon and one-photon excitation are located at about the same position.

3.3 Being a polymer semiconductor

g-C_3N_4 possesses a bandgap of *ca.* 2.7 eV, with the conductive band (CB) and valence band (VB) positions, respectively, at *ca.* −1.1 eV and *ca.* +1.6 eV *vs.* normal hydrogen electrodes (NHEs). This underlines that it can be a visible-light-active photocatalyst for overall water splitting. The suitable electronic band structure also makes carbon nitride a promising candidate for solar energy converting systems, such as photoelectrochemical cells.

3.4 Stability

Thermogravimetric analysis of g-C_3N_4 showed that this material can endure thermally up to 600 °C. A strong endothermal peak appears at 630 °C, paralleled by the consecutive complete weight loss, which indicates that the thermal decomposition and vaporization of the fragments have started at this temperature. The complete decomposition of carbon nitrides occurs up to 750 °C, and no residue of the material is left afterwards. On the one hand, this thermal stability is one of the highest for an organic material, which is fantastic for high temperature applications. The thermal stability of carbon nitride would be slightly different in terms of various preparation procedures, which is caused by the different degrees of condensation. On the other hand, the decomposition temperature is still lower than the graphitization temperature of carbon, which suggests the possibility for acting as templates for synthesizing a refined carbon nanostructure.

The excellent chemical stability against acid corrosion was also revealed in the study of other properties. Zhang and coworkers found out that the dispersion of g-C_3N_4 could form a true solution.[50] The recovered material g-C_3N_4 from acid solution still possessed a predominant (002) peak in the X-ray diffraction spectrum, indicating that g-C_3N_4 could easily restack. In addition, g-C_3N_4 nanosheets or single-layered quantum dots in neutral water are usually negatively charged (with a zeta potential of around −40 mV).[15,51,52] The highly negative surface charge endows the stable suspension of g-C_3N_4 nanostructures in aqueous solution, which could stand still for several weeks without aggregation or precipitation.

3.5 Crystal structure of idealized g-C_3N_4

As is well known, carbon nitrides can exist in several allotropes with diverse properties, and the graphitic phase is regarded as

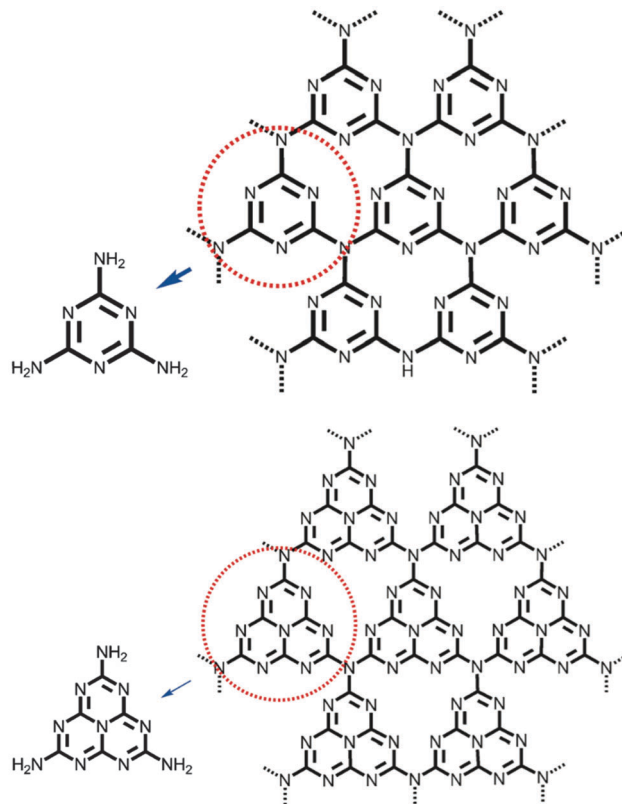Fig. 2 Triazine- (top) and tri-*s*-triazine-based connection patterns (bottom) of potential g-C_3N_4 allotropes. (Adapted with permission from ref. 21. Copyright (2012) the Wiley-VCH.)

the most stable under ambient conditions.[23] Triazine units (C_3N_3) had been proposed as some of the basic building blocks of g-C_3N_4. The other structural models, tri-*s*-triazine (heptazine, C_6N_7) rings, which are structurally close to the Melon structure, are more energetically favored building blocks of g-C_3N_4 than triazine.[23,53] The triazine or tri-*s*-triazine rings are cross-linked by trigonal nitrogen atoms to form extended networks, as seen in Fig. 2.

4. Emerging applications of g-C_3N_4

4.1 g-C_3N_4 based sensing

4.1.1 Sensing relying on luminescence. In industrial and mining areas, large amounts of toxic metal ions have been released into the natural environment, which has raised great concerns over monitoring and detecting related compounds. Chemical sensing using fluorescence to signal a molecular recognition event was firstly demonstrated in the early 1980s. To date, the fluorescence techniques have been seen as important and feasible detection methods, and the literature on that is well developed using various fluorescent probes for various metal ions, including fluorescent metal nanoparticles, organic dyes, and semiconductor or metal quantum dots, and so on.[54] The sensing mechanism is based on the altered probe fluorescence intensity in the presence of the detected ions. Considering the obvious drawbacks of the previous fluorescent probes such as easy oxidation, photobleaching, toxicity, high cost, and potentially

2312 | *Chem. Soc. Rev.*, 2016, **45**, 2308–2326

This journal is © The Royal Society of Chemistry 2016

low photoresponse, it is promising to develop highly fluorescent metal-free nanomaterials with pronounced photostability and low toxicity.

What makes g-C$_3$N$_4$ an ideal candidate for fluorescence sensing is the really extremely stable photoluminescence intensity against photobleaching. Lee *et al.* reported the utilization of g-C$_3$N$_4$ to detect trace amounts of copper metal ions in aqueous solutions. The employed mpg-C$_3$N$_4$ showed highly selective and sensitive photoluminescence quenching response to Cu^{2+} without interference by other metal ions, and the detection limit was determined as 12.3 nM.[12] Given that the nanosheets offer a higher surface-area-to-volume ratio and expose all of its coordination points to metal ions, it is reasonable to develop g-C$_3$N$_4$-nanosheet based fluorosensors for metal ions with an expected even higher detection rate and sensitivity. Tian *et al.* indeed found that ultrathin g-C$_3$N$_4$ nanosheets obtained by ultrasonication-assisted liquid exfoliation could serve as effective fluorescent probes for the sensitive and selective detection of Cu^{2+} with detection limit as low as 0.5 nM.[13] The fluorescence of g-C$_3$N$_4$ nanosheets was quenched by Cu^{2+} *via* a photoinduced electron transfer, as the redox potential of Cu^{2+}/Cu$^+$ lies in between the CB and the VB of g-C$_3$N$_4$. They further made a test paper with a naked-eye detection limit of 0.1 nM and expanded the g-C$_3$N$_4$ based sensing systems by developing a highly sensitive glucose optical detector based on the same fluorescence quenching mechanism.[55] In addition, g-C$_3$N$_4$ based sensing has also been extended to Fe^{3+}, heparin, Pb^{2+}, Hg^{2+}, and Cr^{6+}, based on the same sensing mechanism.[45,56,57]

Different from the fluorescence quenching detection mechanism indicated above, Zhang *et al.* expanded the g-C$_3$N$_4$ based sensing by developing a turn-on fluorescent sensor based on the g-C$_3$N$_4$/MnO$_2$ composite, as illustrated in Fig. 3.[58] The fluorescence of g-C$_3$N$_4$

was firstly quenched by the sandwiched MnO$_2$, while the to-be-tested glutathione molecule could restore the fluorescence by eliminating electron transfer from g-C$_3$N$_4$ to MnO$_2$. The detection limit for the glutathione molecule was determined to be 0.2 μM under optimal conditions. The authors further successfully applied the developed sensor for visualizing and monitoring the change of intracellular glutathione in living cells.

g-C$_3$N$_4$ was found to be able to quench the fluorescence of fluorophores labeled on DNA, which is different from the previously reported label-free sensing. Based on the investigation of the interaction between DNA and g-C$_3$N$_4$, Wang *et al.* found that the strong affinity between single-stranded DNA (ssDNA) and g-C$_3$N$_4$ led to a fast fluorescence-quenching phenomenon through the photoinduced electron which transfers from the excited fluorophore to the conductive band of g-C$_3$N$_4$ nanosheets (Fig. 4).[14] Utilizing the affinity change of g-C$_3$N$_4$ nanosheets toward ssDNA probes upon the specific recognition of target analytes (such as RNA, proteins, small molecules and some ions), the quenching effect has been employed to design a universal strategy for homogeneous fluorescence based sensing.

The investigation of chemiluminescence behavior of g-C$_3$N$_4$ with different co-reactants provides another effective way for developing g-C$_3$N$_4$ based luminescent sensors. Cheng *et al.* reported the cathodic electrogenerated chemiluminescence (ECL) behavior of g-C$_3$N$_4$ with K$_2$S$_2$O$_8$ as a coreactant, as illustrated in Fig. 5. The electrochemically reduced g-C$_3$N$_4$ (g-C$_3$N$_4$$^{\bullet-}$) formed by the injected electron from the electrode could react with K$_2$S$_2$O$_8$ to generate a cathodic ECL. Though the formation of an excited state of g-C$_3$N$_4$ in electrogenerated chemiluminescence is different from the direct bandgap excitation in photoluminescence, the maximum emission of both types of luminescence is situated at the same wavelength, suggesting that identical excited states
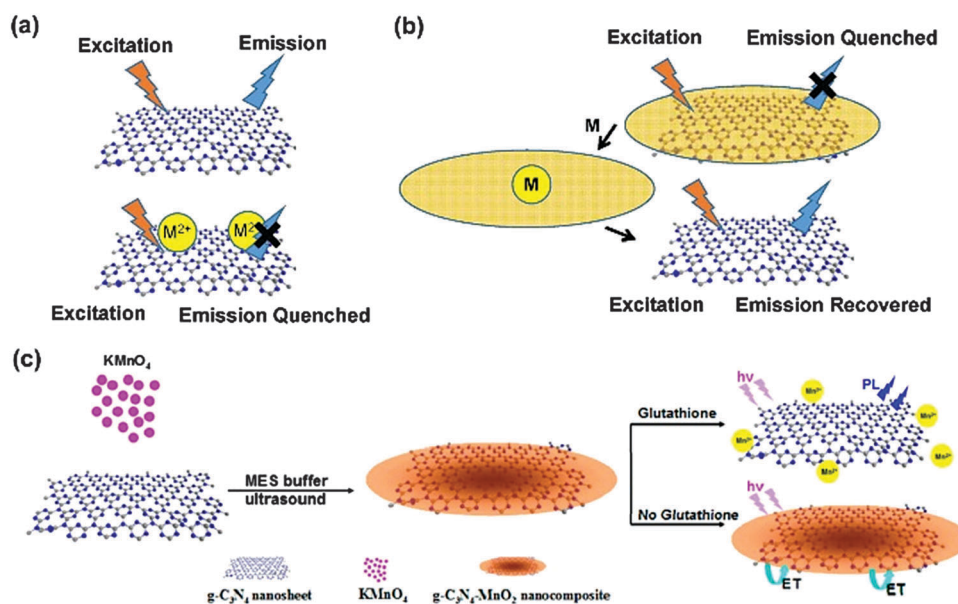

Fig. 3   (a) Fluorescence on and off for sensing based on pristine g-C$_3$N$_4$. (b) Fluorescence off and on for sensing based on the g-C$_3$N$_4$ composite. (c) Schematic representation of the g-C$_3$N$_4$–MnO$_2$ nanocomposite for sensing of glutathione. (Adapted with permission from ref. 58. Copyright (2014) American Chemical Society.)
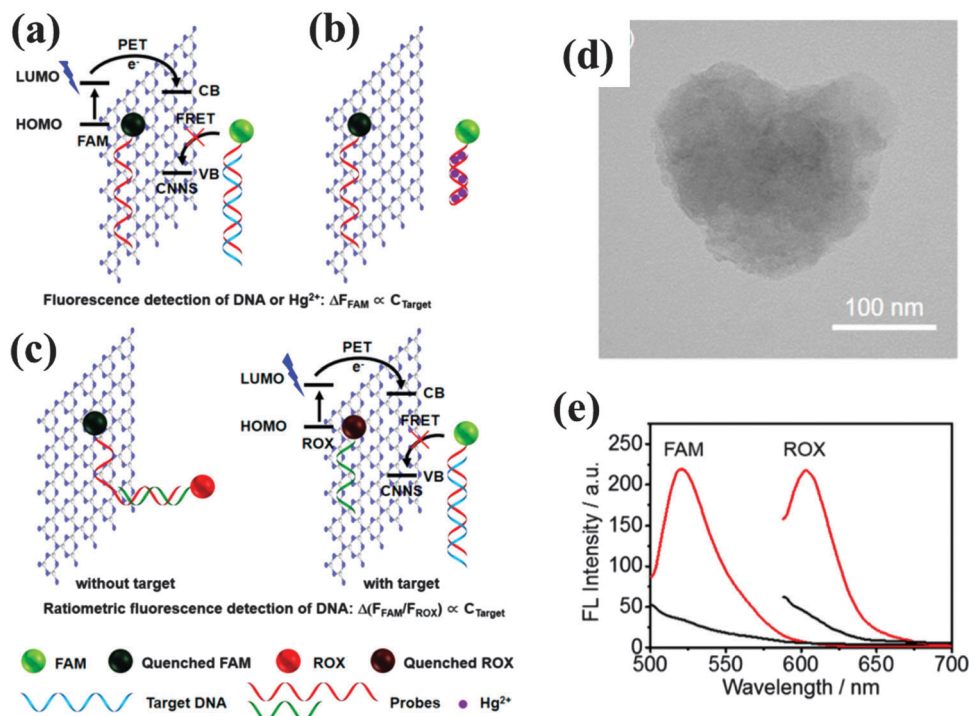
Fig. 4 Schematic illustration of the interaction of DNA with g-C$_3$N$_4$ nanosheets, fluorescence quenching mechanism of g-C$_3$N$_4$ nanosheets, and sensing strategy for the fluorescence detection of (a) DNA and (b) Hg^{2+} and (c) ratiometric fluorescence detection of DNA. (d) TEM image of the as-exfoliated g-C$_3$N$_4$ nanosheet. (e) Fluorescence spectra of 10 nM probe 1 (left) and probe 2 (right) in the absence (red) and the presence (black) of 15 μg mL^{-1} of g-C$_3$N$_4$ nanosheet. (Adapted with permission from ref. 14. Copyright (2013) American Chemical Society.)

are generated.[16] The cathodic ECL of g-C$_3$N$_4$ was used to detect Cu^{2+}, with a limit of detection at 0.9 nM. Likewise, anodic ECL could also be established.[49] Liu *et al.* also utilized anodic ECL with a g-C$_3$N$_4$ nanosheet electrode to sense dopamine based on the same fluorescence quenching mechanism.[59]

4.1.2 Sensing based on electrochemistry. N-doped carbons have received considerable attention due to the strong electron donor nature of nitrogen which should enhance the collective π bonding, leading to the improved stability, electron transfer rate, and hence durability of the carbon supports during electrocatalytic processes.

In general, N-doping can be achieved by either "post-doping", namely post-synthesis treatment of carbons by N-containing chemicals, or *in situ* doping, *i.e.*, direct synthesis of nanostructured carbons involving N-containing precursors. In this regard, carbon nitride, a carbon-like material that is highly enriched with nitrogen and that can be readily obtained through the condensation of cyanamide, may also serve as a potential component and a nitrification agent for electrochemical applications.

Zhang *et al.* synthesized the two-dimensional mpg-C$_3$N$_4$ and utilized the obtained material as a nitrification agent for an
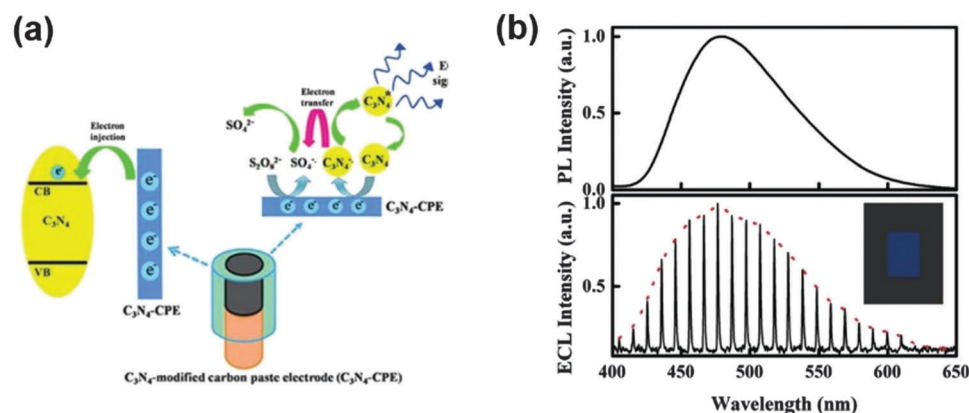

Fig. 5 (a) The schematic illustration for the ECL process. (b) Top figure shows the PL spectrum of g-C$_3$N$_4$ solid powder when excited at 365 nm and bottom figure shows the ECL spectrum of the g-C$_3$N$_4$-modified electrode in 0.10 M K$_2$SO$_4$ containing 3.0 mM K$_2$S$_2$O$_8$ by cycling the potential between 0.00 and −1.30 V (*vs.* Ag/AgCl) with 1 mV step potential. (Adapted with permission from ref. 16. Copyright (2012) American Chemical Society.)

electrochemical sensing platform for H$_2$O$_2$, nitrobenzene, and NADH detection, respectively.[60] The researchers found out that the relative amounts of N-bonded species (pyridinic N, pyrrolic N, and graphitic N) depend on the different pyrolysis temperatures. The ratios among the three N-bonding configurations are thought to affect the electrochemical performance. Pyridinic N atoms with strong electron-accepting ability could create a net positive charge on the adjacent carbon atoms in the carbonaceous residues of g-C$_3$N$_4$, which are favorable for the adsorption of small molecules (e.g., H$_2$O$_2$, nicotinamide adenine dinucleotide, abbreviated as NADH, and nitrobenzene) and can readily transfer electrons from the anode, thus facilitating the electrochemical reaction. The detection range for these different probe molecules is summarized in Table 1.

The morphology of the g-C$_3$N$_4$ materials affects their electrochemical performance. Structuring g-C$_3$N$_4$ into a nanosheet by sonication delamination, Xu et al. fabricated a g-C$_3$N$_4$ nanosheet based electrode and constructed a photoelectrochemical sensor.[61] They found that the photocurrent of the g-C$_3$N$_4$ modified indium tin oxide (abbreviated as ITO) electrode was obviously enhanced after adding Cu^{2+}. They claimed that a good linear relationship could be obtained between the photocurrent increase and the concentration of Cu^{2+} over the range from 0 to 7.6 μM. The photocurrent enhancement was ascribed to the electron accepting character of Cu^{2+}, which was thought to contribute to an improved electron/hole separation occurring on the g-C$_3$N$_4$ nanosheet electrode under illumination.

In terms of the moderate conductivity of g-C$_3$N$_4$, which unfortunately limits its application and greatly affects its performance in the field of electrochemistry, composite formation is advised for better performance and more diverse applications. A nanocomposite made up of ultrathin g-C$_3$N$_4$ and TiO$_2$ was utilized as a sensing element in a photoelectrochemical platform with a thin layer structured flow-cell configuration for real-time evaluation of global antioxidant capacity (Fig. 6).[62] It was found that the combination of the nanosheet and the nanoparticle outperformed the single component in terms of optoelectronic function performances. The photoelectrochemical platform could fully overcome the major interference or poisoning problems that other antioxidant capacity assays usually suffered from while also featuring advantages such as rapid response time, high sensitivity, long-lasting stability and minimal sample requirement. Dong and coworkers developed a electrochemical

humidity sensor (as shown in Fig. 7) based on Li$^+$ intercalated g-C$_3$N$_4$ nanosheets.[63] They attributed the ultrafast response and recovery time to the unique two-dimensionally intercalated structure in which Li species linked with nitrogen of g-C$_3$N$_4$ could make protons conductive in the first adsorbed water layer. The response and recovery time of the g-C$_3$N$_4$ sensor outperformed most of the traditional oxide ceramic-based sensors under similar testing conditions.

Since g-C$_3$N$_4$ can be considered as an analogue of graphite with N substitution, the interaction between graphene and g-C$_3$N$_4$ nanostructures, especially nanosheets, is highly promising. As described by Du et al., the strong electronic coupling of g-C$_3$N$_4$ and graphene and the charge transfer at the graphene/g-C$_3$N$_4$ interface enhance the electron conductivity of g-C$_3$N$_4$.[64] Based on such heterojunction concepts, Zheng et al. found that the coupling of these two layered materials resulted in comparable or even better performance in electrocatalytic hydrogen evolution reaction than that of traditionally chosen metals.[9] Hu et al. found out that by employing differential pulse voltammetry, a g-C$_3$N$_4$ nanosheet/graphene oxide (GO) composite modified electrode exhibits distinguished electrocatalytic activity towards the oxidation of ascorbic acid, dopamine and uric acid, respectively, but could also be used for the detection of urine.[65]

In addition to the fluorescence "on/off" mechanism mediated by g-C$_3$N$_4$ and its composites, the sensing can also be feasibly based on adsorption. Jia et al. developed hierarchically ordered macro-/mesostructured g-C$_3$N$_4$ films by using a combination of the P123 block copolymer and monodispersed polystyrene spheres as dual templates.[36] The obtained pristine g-C$_3$N$_4$ film showed excellent adsorption capability for acidic molecules. Interestingly, the adsorption properties can be reverted by a simple treatment with UV light and oxygen that generates COOH and N-oxide groups on the surface, which tune the adsorption selectivity to basic molecules.

To give readers a scenario of how g-C$_3$N$_4$ based sensors are progressing, Table 1 is illustrated to summarize briefly the overall sensing parameters including the sensing probe, response time, linear range, and detection limit that those state-of-the-art sensors have achieved.

4.2 g-C$_3$N$_4$ in biomedical applications

A biocompatible material should satisfy the requirements of biosafety (no negative responses) and biofunctionality (ability to

Table 1 g-C$_3$N$_4$ based structures for sensing

| g-C$_3$N$_4$ structures	Synthesis	Probe	Detection limit	Linear range	Response time	Mechanism	Ref.
c-mpg	Template	Cu^{2+}	12.3 nM	10–100 nM		Fluorescence quenching	7
CNSs	Sonication	Cu^{2+}	0.5 nM	0–1 × 10^4	10 min	Fluorescence quenching	40
Fe–CNSs	Sonication	H$_2$O$_2$	0.05 μM	5 × 10^{-7} ~1 × 10^{-5} M	1 min	Optical absorbance	41
		Glucose	0.5 μM				
CNSs	—	Heparin	18 ng mL^{-1}	0.05–5 μg mL^{-1}	2 hours	Fluorescence quenching	43
g-C$_3$N$_4$/MnO$_2$	Post-treatment	Glutathione	0.2 μM	0–250 μM	6 s	Fluorescence recovery	44
g-C$_3$N$_4$/carbon	Post-treatment	Cu^{2+}	0.9 nM	2.5–100 nM	200 s	Chemiluminescence quenching	35
CNS/C	Post-treatment	Dopamine	96 pM	1.0 nM to 100 nM	30 s	Chemiluminescence quenching	46
g-C$_3$N$_4$ NS	Sonication	DNA, Hg^{2+}	2.1 nM	3.0–30 nM	30 min	Fluorescence quenching	45
g-C$_3$N$_4$ film	Template	Acid/basic molecules	—	—	—	Adsorption	22
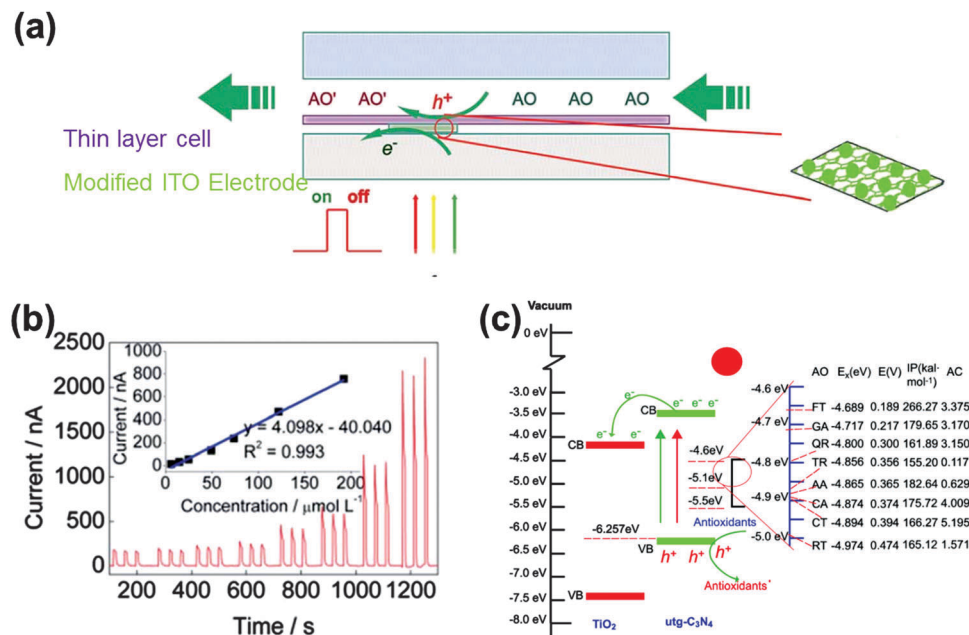
Fig. 6 (a) Illustration of the thin layer photoelectrochemical flow cell. (b) Concentration-dependent photocurrent of one of the antioxidants (caffeic acid). (c) Mechanism of the photoelectrochemical sensor for the detection of the antioxidant capacity. (Reproduced from ref. 62 with permission from the Royal Society of Chemistry.)
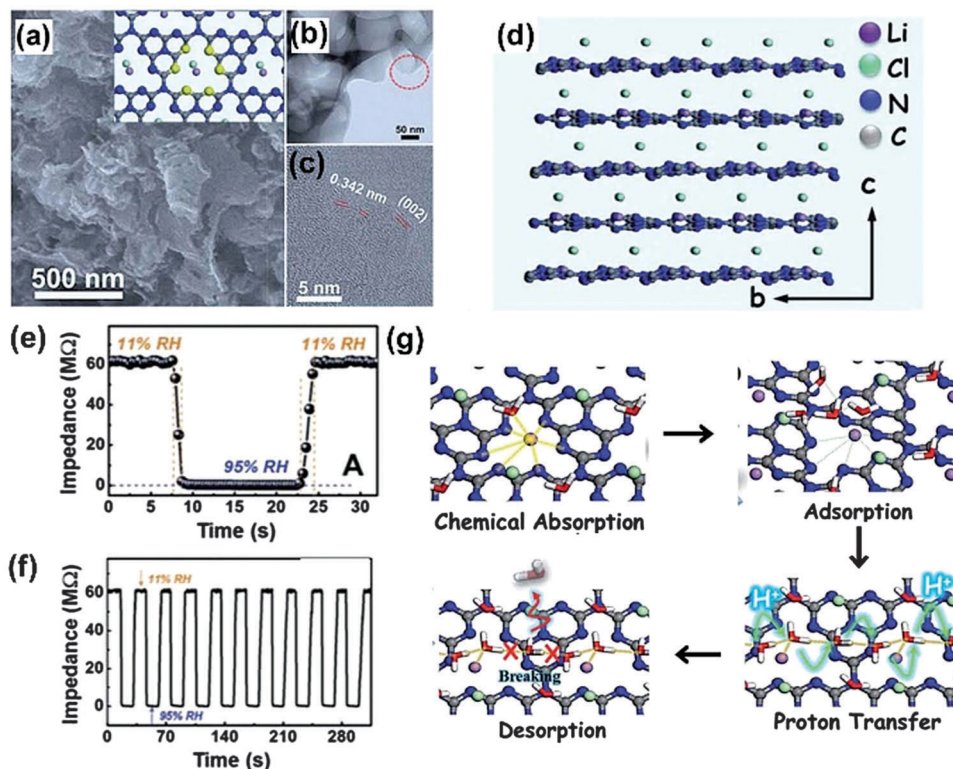

Fig. 7 (a) SEM image of LiCl-intercalated g-C$_3$N$_4$; TEM (b) and high-resolution TEM (c) of LiCl-intercalated g-C$_3$N$_4$. (d) The side view of the crystallographic structure model of a perfect LiCl-intercalated g-C$_3$N$_4$. Response and recovery characteristic curves based on the nanosensor containing LiCl-intercalated g-C$_3$N$_4$ for 1 cycle (e) and 10 cycles (f). (g) The theoretical calculation results showing the water adsorption and desorption process on the surface of LiCl-intercalated g-C$_3$N$_4$. (Reproduced from ref. 63 with permission from the Royal Society of Chemistry.)

perform a designed task).[66] Benefiting from the inherent blue light photoluminenscence with high quantum yields, high

stability and good biocompatibility, g-C$_3$N$_4$ meets the above requirements. Therefore, g-C$_3$N$_4$ can be studied as a platform

2316 | *Chem. Soc. Rev.*, 2016, **45**, 2308–2326

This journal is © The Royal Society of Chemistry 2016

for bio-related applications, and actually, it is already becoming an important candidate for bioimaging application.

Zhang *et al.* carried out first-principles density-functional calculations to study the electronic structure of the bulk and g-C_3N_4 nanosheet, respectively (as illustrated in Fig. 8).[17]

The calculated density of states (DOS) of single-layered g-C_3N_4 nanosheets shows an obvious increase at the conduction band edge with respect to the bulk counterpart, indicating that the atomically thick g-C_3N_4 nanosheets possess more charge carriers. Therefore, it is anticipated that the two-dimensional ultrathin
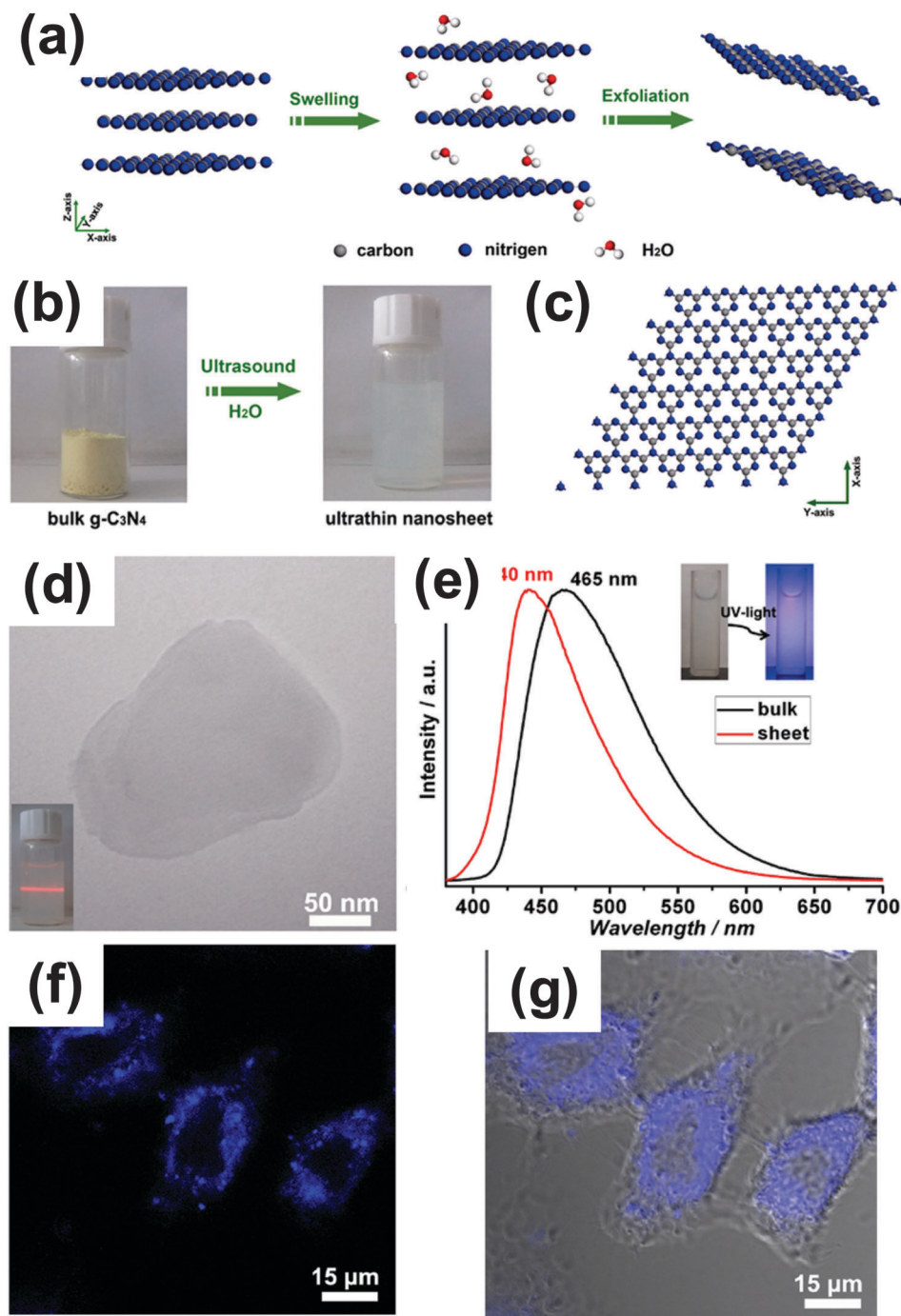

Fig. 8 (a) Schematic illustration of the liquid-exfoliation process from bulk g-C_3N_4 to ultrathin nanosheets. (b) Photograph of bulk g-C_3N_4 and suspension of ultrathin g-C_3N_4 nanosheets. (c) A theoretically perfect crystal structure of g-C_3N_4 projected along the z-axis. (d) TEM image of the ultrathin g-C_3N_4 nanosheet; the inset of (a) is the Tyndall effect of the ultrathin g-C_3N_4 nanosheet dispersed in water. (e) Normalized photoluminescence spectra of bulk g-C_3N_4 and ultrathin g-C_3N_4 nanosheets. (f) Confocal fluorescence image and (g) overlay image of bright field and confocal fluorescence images of the HeLa cells incubated with ultrathin g-C_3N_4 nanosheets for about 1 h. (Adapted with permission from ref. 17. Copyright (2012) American Chemical Society.)

This journal is © The Royal Society of Chemistry 2016

Chem. Soc. Rev., 2016, **45**, 2308–2326 | **2317**

g-C_3N_4 nanosheets show improved response compared to the bulk counterpart. The cell biocompatibility experiment indicated that with the incubated nanosheet concentration up to 600 μg mL^{-1}, HeLa cells did not lose cell activity and could maintain their normal morphology, suggesting an excellent biocompatibility of the g-C_3N_4 nanosheets.[17] The confocal fluorescence microscopy tests thereby demonstrated that unfunctionalized ultrathin g-C_3N_4 nanosheets could be used as promising biomarkers for the labeling of the cell's membranes. They further found out that g-C_3N_4 in such situations could undergo two-photon absorption (TPA), which opens the possibility of employing g-C_3N_4 as a TPA probe. In two-photon fluorescence bioimaging, it was shown that g-C_3N_4 quantum dots could effectively pass through the nuclear pore complex and penetrate into the nuclei. Compared with one photon fluorescence imaging, the two photon fluorescence imaging with g-C_3N_4 QD allowed us to sharply distinguish the position and details of the cell nuclei.[15]

g-C_3N_4 nanosheets could also serve as potential photosensitizers and pH-responsive drug nanocarriers for cancer imaging and therapy.[67] Unlike many conventional sensitizers which suffer from poor solubility in water, photobleaching phenomena and low selectivity, g-C_3N_4 nanosheets are capable of generating reactive oxygen species for killing cancer cells efficiently under low-intensity light irradiation (20 mW cm^{-2}). The nanosheets herein could also be used as nanocarriers for loading the anticancer drug doxorubicin (DOX), and the release could be triggered by pH changes. In addition, due to the high surface-to-volume ratio, g-C_3N_4 nanosheets bear an ultrahigh capacity for DOX loading. Interestingly, the fluorescence of g-C_3N_4 nanosheets enabled the direct visualization of the delivery process of DOX.

Tang and coworkers used g-C_3N_4 nanosheets synthesized from pyrolysis of guanidine hydrochloride as probes for *in vitro* imaging of biothiols (cysteine, homocysteine, and glutathione) in biological fluids. They found that these g-C_3N_4 materials exhibited an intense, long-persistent luminescence even after the removal of the excitation source.[68] Ag$^+$ ions were used to quench the persistent luminescence of g-C_3N_4 *via* electron transfer, and the persistent luminescence could be switched on again by interrupting the quenching interaction between g-C_3N_4 and Ag$^+$ through the addition of biothiols. The strong and specific affinity of biothiols to Ag$^+$ results in the desorption of Ag$^+$ from the g-C_3N_4 surface, which explained the recovery of the persistent luminescence. According to the authors, it is possible to observe the sensing capability by measuring the afterglow image using CCD imaging.

4.3 g-C_3N_4 for novel solar energy exploitation

g-C_3N_4 is capable of catalyzing hydrogen/oxygen evolution and CO_2 reduction under bandgap excitation and in the presence of suitable cocatalysts and/or sacrificial agents. It was found that the g-C_3N_4 based composite such as g-C_3N_4/C or g-C_3N_4/polypyrrole could directly split water under visible light irradiation, which can be seen as the mandatory next step.[8,69] However, the conversion of light to fuel, with fuels being usually a low value commodity, at an affordable price and on a large scale is still a long-range goal. On the long journey to fulfill the challenging goal of

artificial photosynthesis, the photogenerated electron or hole could be possibly used more valuably and efficiently by integrating photochemistry with other established conventional systems striving for high value synthesis.

For instance, cofactor (NADH or FAD) regeneration is important for sustainable enzymatic synthesis, especially when considering that the interest of applying enzymes in organic synthesis is increasing. Compared with the conventional electrochemical or enzymatic regeneration, the photocatalytic regeneration method is promising in the view of using light as the only input. Inspired by the photosynthesis in diatoms, a g-C_3N_4 based diatom frustule membrane reactor was recently developed for NADH regeneration in the presence of [Cp*Rh(bpy)Cl]Cl as an electron and proton mediator, as illustrated in Fig. 9. The photochemically regenerated NADH could be used to feed enzymatic reactions.[47] The *in situ* NADH regeneration rate is high enough to reverse the biological pathway of the three consecutive dehydrogenase enzymes (formate dehydrogenase, formaldehyde dehydrogenase, and alcohol dehydrogenase, respectively), which allows for instance the successive conversion of formaldehyde to methanol and also the reduction of carbon dioxide to methanol.[38] Liu and coworkers further developed a sacrificial templating route for constructing mesoporous g-C_3N_4 spheres and a high-throughput method for the synthesis of nanostructured g-C_3N_4 rods, which are superior for NADH regeneration (Fig. 9a–c). An *in situ* enzymatic scheme for amino acid synthesis could be realized (Fig. 9d–f).[27,70] Recently, they extended the photocatalytic route to the indirect electrochemical regeneration of NADH by using ultrathin g-C_3N_4 film electrodes and a rather conventional [Cp*Rh(bpy)Cl]Cl complex.[71] There are however some key issues to be solved prior to practical applications of the photocatalytic cofactor regeneration system, such as mediator immobilization and the exploration of a noble metal-free mediator system.

The photocatalytic production of hydrogen peroxide (H_2O_2) on semiconductor catalysts with alcohol and O_2 is regarded as promising for safe and green H_2O_2 synthesis. The photocatalytic process could avoid the use of explosive H_2/O_2 mixed gases in the direct synthesis. The previously reported photocatalytic systems produced H_2O_2 usually with poor selectivity (~1%). Shiraishi *et al.* reported that g-C_3N_4 efficiently produced H_2O_2 with very high selectivity up to 90% in an alcohol/water mixture with O_2 under visible light irradiation ($\lambda > 420$ nm).[72] Raman spectroscopy and electron spin resonance analysis revealed that the high H_2O_2 selectivity was due to the efficient formation of 1,4-endoperoxide species on the g-C_3N_4 surface. One-electron reduction of O_2 (superoxide radical formation) was suppressed, enabling the selective promotion of H_2O_2 formation (two-electron reduction of O_2).[73] The enormous defects in larger surface area mpg-C_3N_4 could act as the active sites for the four-electron reduction of O_2 (instead of two-electron reduction) and also for the photocatalytic decomposition of H_2O_2. Therefore, to maximize the H_2O_2 formation with high activity and selectivity, g-C_3N_4 catalysts should possess a relatively large surface area but minimal surface defects.

Kiskan *et al.* reported the first successful use of mpg-C_3N_4 as a visible light photoinitiator in the free radical polymerization
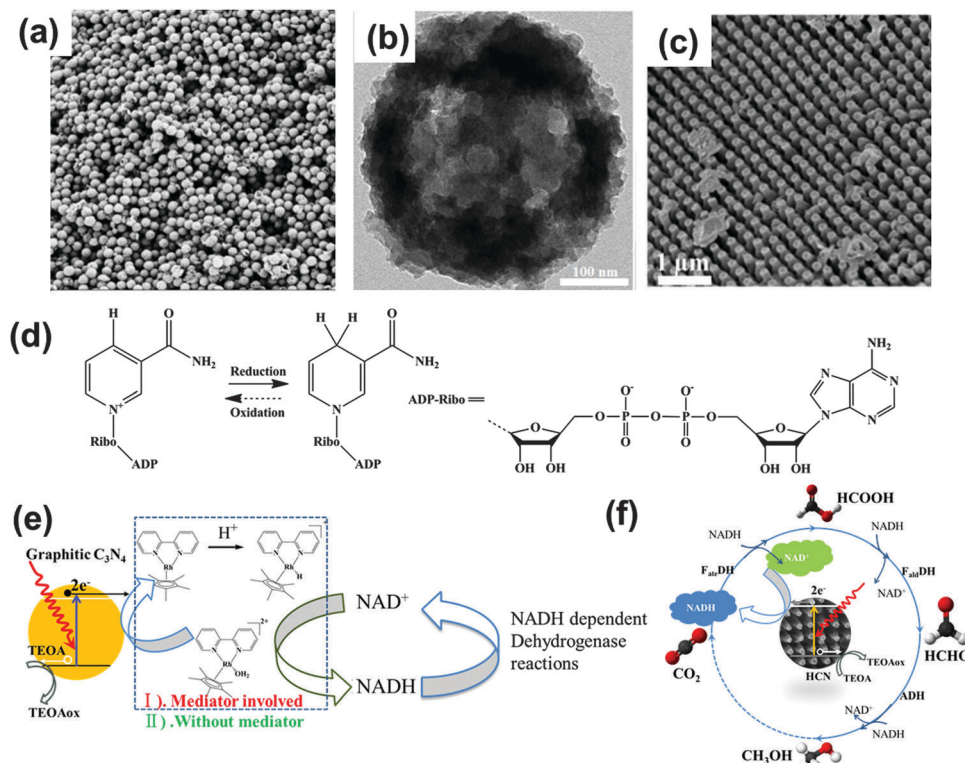
Fig. 9 (a) Illustration of a perfect graphitic carbon nitride constructed from heptazine building blocks. (b and c) g-C_3N_4 based array and mesoporous sphere for photocatalytic NADH regeneration for *in situ* enzymatic reactions. (d) Redox equilibrium between β-NAD^+ and NADH. Schematic illustrations of one enzymatic reaction of H_2O_2 reduction (e) and three consecutive enzymatic reactions for converting CO_2 into methanol (f) with *in situ* regeneration of NADH by g-C_3N_4 photocatalysis. (Ref. 27, 38 and 47 – Published by The Royal Society of Chemistry.)

of vinyl monomers such as methyl methacrylate.[74] They showed that mpg-C_3N_4 exhibits excellent performance in the initiation and can easily be separated from the polymerization mixture and reused without a significant loss of the activity. However, triethanolamine was still needed to close the light driven radical initiation step. The current paper's authors recently found out that the exfoliated layered g-C_3N_4 itself could initiate the radical polymerization of *N*-isopropylacrylamide (abbreviated as NIPAAM) into a hydrogel. This process works similar to the TiO_2 nanosheets reported by Liu and Aida *et al.*[75] The obtained PNIPAAM hydrogel possesses temperature responsive properties. In this case, the amines employed in Kiskan's work that act as the sacrificial agent are not necessary, as water as such is activated. Woznica *et al.* found out that mpg-C_3N_4 was found to be an efficient heterogeneous photocatalyst for the radical cyclization of 2-bromo-1,3-dicarbonyl compounds to functionalized cyclopentanes under mild conditions. This reaction performed in THF can be conducted in a continuous flow photoreactor with THF playing the role of solvent and crucial proton and electron donors as well.[76]

It was demonstrated that the yellow carbon nitride powder could also kill bacteria under illumination, which is already well known for TiO_2 photocatalysis,[77] however now moved into the more appropriate visible light range. Huang *et al.* demonstrated that g-C_3N_4 could be employed as a metal-free catalyst for the inactivation of *Escherichia coli* K-12 (*E. coli*), a common

Gram-negative bacterium, under visible light illumination.[78] The authors explained that the oxidative pathway *via* the positive holes is dominant in the bacterial inactivation by carbon nitride photocatalysis. g-C_3N_4 could also be coupled with conventional Ag nanoparticles to enhance the antibacterial and biofilm elimination activity.[79]

4.4 Devices of g-C_3N_4

Two-dimensional materials are fascinating.[80] As the "infinite" extension of two-dimensional nanosheets, assembling g-C_3N_4 in the form of a film is crucial as it is an important step toward integrating its favorable properties and performance into a device. The straightforward way would be to place the pre-synthesized graphitic carbon nitride powder on desired substrates by coating techniques such as spin coating, and then sintering the sample. This is technically simple but has serious limitations in terms of film homogeneity, lamellar orientation, and accessing more elaborate sub-structures, and the practically realized structures up to now are usually not satisfactory or favorable for good device performance.[30,81] Techniques relying on physical deposition such as pulsed laser deposition are able to produce high quality films of carbon nitride, while the cost induced by the valuable instruments has to be considered for the real commercialization.

Basically, two ways for synthesizing g-C_3N_4 based films can be differentiated: post-powder processing and *in situ* growth.

This journal is © The Royal Society of Chemistry 2016

Chem. Soc. Rev., 2016, 45, 2308–2326 | 2319

The post-powder processing refers to the possibility of employing the as-formed nanostructures for film formation. Zhang *et al.* fabricated a g-C_3N_4 film by depositing the as-exfoliated g-C_3N_4 nanosheet into a cellulose membrane by vacuum filtration while a free-standing g-C_3N_4 film could be obtained after dissolving the cellulose membrane template in acetone (Fig. 10a–c).[17] The film was thought to be transferrable to other conductive substrates. Zhang *et al.* adopted a more harsh condition to process as-formed g-C_3N_4 for film formation (Fig. 10d and e).[82] They found that the chemical protonation of graphitic carbon nitride solids with nitric acid could result in a stable carbon nitride colloidal suspension, which can be processed into thin films by conventional dip/disperse-coating techniques. At the same time, Zhang *et al.* found out that g-C_3N_4 could dissolve in concentrated sulfuric acid with concentration up to 300 mg mL^{-1}, which could also enable film formation.[50]

Recently, some report about *in situ* growth of g-C_3N_4 films in the presence of substrates came into the view. Xu *et al.* reported a liquid-mediated pathway for the growth of continuous polymeric carbon nitride thin films on several substrates, including FTO, TiO_2, molybdenum and aluminum foil.[18] Typically, they placed an adequate amount of dried precursor powder into a crucible, totally covering the substrate placed at the crucible bottom. The crucible was then covered with a lid and heated at 550 °C for 4 h in a nitrogen atmosphere.

Aida *et al.* invented a evaporation technique for growing g-C_3N_4 based films on different substrates (Fig. 10f).[83] Liu *et al.* developed an economic and facile nanoconfinement method to fabricate a patterned graphitic carbon nitride film (Fig. 10g–i).[34] An "ink" (cyanamide) infiltrated anodic aluminum oxide stamp is found to be capable of "ink-jetting" carbon nitride films featuring regular microstructures of the stamp onto the substrates *via in situ* "chemical vapor deposition". A photocurrent density of 30.2 μA cm^{-2} at 1.23 V_{RHE} is achieved for such a film printed on a conductive substrate. Besides the good photocurrent, the film grown on a normal glass slide could be peeled off from the substrate by immersing the whole glass inside water. As illustrated in Fig. 10h, the peeled whole piece of film floats on the water surface. Amazingly, due to the regular and periodic structure of the porous AAO template, the as-obtained film could possess a structural color and could be processed as a two-dimensional photonic crystal, adding to the functionality of the film.
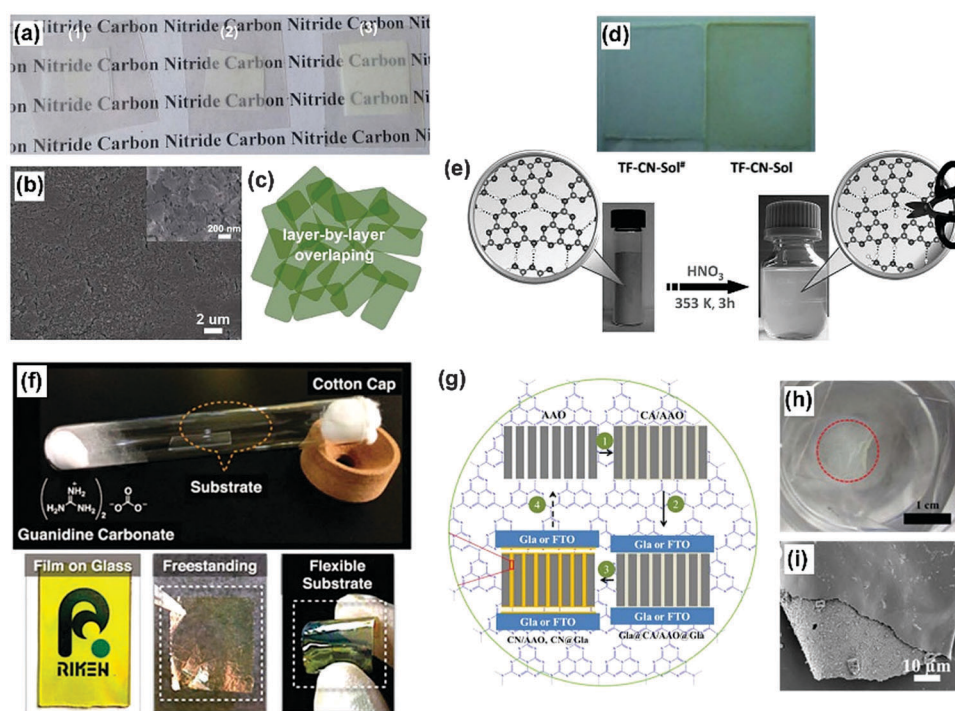

Fig. 10 (a–c) Photograph of g-C_3N_4 nanosheet films with different thicknesses transferred onto a plastic substrate, showing transparent character, SEM image of the surface morphology for the thin film assembled from g-C_3N_4 nanosheets and schematic illustration of the layer-by-layer overlapping structure of assembled ultrathin g-C_3N_4 nanosheets. (d and e) The chemical protonation of graphitic carbon nitride solids with nitric acid could result in a stable carbon nitride colloidal suspension, which can be processed into thin films by conventional dip/disperse-coating techniques. (f) The evaporation technique for growing g-C_3N_4 based films on different substrates. (g–i) Schematic illustration of printing graphitic carbon nitride films on "sandwiching" substrates. The whole process includes four steps: (1) infiltration of the "ink" of cyanamide in AAO (inking the stamp); (2) sandwiching AAO with two substrates (applying the stamp to the substrates); (3) printing graphitic carbon nitride films on "sandwiching" substrates by the thermal condensation of cyanamide in a confined environment at 550 °C (printing the stamp onto the substrates *via in situ* nanoconfinement growth); (4) decomposition process by calcination in air to remove the CN residue on the AAO for its recycle (recycling the stamp). (Adapted with permission from ref. 17. Copyright (2012) American Chemical Society; adapted with permission from ref. 82. Copyright (2015) the Wiley-VCH; adapted with permission from ref. 34. Copyright (2015) the Wiley-VCH.)

2320 | *Chem. Soc. Rev.*, 2016, **45**, 2308–2326

This journal is © The Royal Society of Chemistry 2016

The visible-light-driven photoresponse could add possibility to the electrochemistry of g-C_3N_4. Zhang *et al.* observed that polymeric carbon nitrides have a photovoltaic effect and are promising in solar energy conversion.[81] They fabricated the nanostructured solid n/p mixtures including ITO/PEDOT-PSS/mpg-C_3N_4 and ITO/mpg-C_3N_4/TiO_2 and the photocurrent was greatly boosted to 90 and 150 μA cm^{-2}, respectively, indicating that the light-generated excitons were more effectively dissociated in both cases. g-C_3N_4 exhibited reasonable efficiency as well as other merits including low cost, facility for mass-synthesis/chemical modification, and, in particular, in contrast to many other organic semiconductors, a high chemical stability against oxidation (stable in air up to 550 °C). However, considering the not-optimized device layout (specifically poor film quality) and the thereby low photocurrent and open-circuit voltage, the work was viewed as "proof of concept" even by the authors themselves.

Xu *et al.* employed a liquid-mediated pathway solution to fabricate a relatively good-quality carbon nitride film and incorporated the as-obtained g-C_3N_4 film into organic solar cells to behave as an electron acceptor in combination with P3HT, obtaining an open-circuit voltage of more than 1 V.[18] The rather low short-circuit current and overall low efficiency however indicated that the device was not optimized. The exploration of photovoltaics nevertheless allows opening up a new application aspect. The same authors also fabricated simple organic light-emitting diodes with the carbon nitride layer sandwiched between a glass/ITO substrate and a Ca/Al top electrode.[84] However, they found a strong redshift for the electroluminescence compared with the photoluminescence, which they ascribed to the disorder of the film and the dominant emission from such defect sites.

Due to the synergistic effects of layer-by-layer structures *via* π–π stacking and/or charge-transfer interactions, g-C_3N_4 nanosheets/GO composites show improved conductivity, electro-catalytic and selective oxidation performance. Inspired by the successful examples of graphene oxide as the active insulator in memory diodes, Zhao *et al.* found out that an atomically thick g-C_3N_4 nanosheet was also capable of acting as the active insulator layer for memory devices.[20] Employing graphene as the electrode, the as-fabricated g-C_3N_4 based memory device shows nonvolatile electrical bistability and a rewritable memory effect with a reliable ON/OFF ratio of up to 10^5.

4.5 g-C_3N_4 as a structuring agent

Nanotemplates, as versatile crafting blueprints, have been widely used in nanomaterial architecture and texture fabrication. A good template could easily define the formation of a nanostructure while it does not disturb the local bonding motifs of the final substance. Nanostructured g-C_3N_4 was fabricated by using different hard and soft templates, as described above. Interestingly, g-C_3N_4 itself could also act as a structuring agent, either as a sacrificial "hard" (refers to preformed g-C_3N_4 nanostructures) or "soft" (refers here to an *in situ* generated g-C_3N_4) template for synthesizing desired architectures. The extraordinary thermal behavior easily allows the removal of g-C_3N_4

after or during the templating process by simply increasing the calcination temperature beyond 600 °C, while the carbon nitride templates are rather stable below the decomposition temperature. In addition to the nanostructure confinement effect, g-C_3N_4 could also simultaneously provide the C and N source for further chemical conversions, respectively.

Large-scale synthesis of nitrogen-rich carbon nitride microfibers could be achieved by the thermal evaporation of graphitic carbon nitride.[40] Due to the high thermal stability of the g-C_3N_4 precursor, it gradually sublimed and produced a constant CN_x ($x > 1$) vapor pressure, which is not only important for the large-scale formation of one-dimensional structures, but also for achieving a large length/diameter ratio of the desired microfibers (Fig. 11). Fischer *et al.* showed that mpg-C_3N_4 can act as both the confinement template and the nitrogen source for the preparation of metal nitride nanoparticles.[85] Starting from the SiO_2 template, two-step replication was adopted to fabricate the desired metal nitride nanoparticles *via* an intermediary negative mpg-C_3N_4 replica. The morphology of the final metal nitride nanostructures was a close but slightly smaller copy of the original SiO_2 template. Using this approach, ternary metal nitride particles with diameters smaller than 10 nm composed of aluminum gallium nitride and titanium vanadium nitride were synthesized, respectively.[86] Due to the confinement effect of the carbon nitride matrix, the composition of the resulting metal nitride can be easily adjusted by changing the concentration of the preceding precursor solution. Thus, rather unconventional ternary metal nitride nanoparticles with continuously adjustable metal composition can also be produced.

By using g-C_3N_4 as the soft template, Gao *et al.* reported the SiO_2-assisted synthesis of TaON over Ta_3N_5 nanoparticles with tailored composition through the calcination of Ta–urea gels with desired urea/Ta ratios, which could be employed for alkene epoxidation.[87] Urea was converted into carbon nitride (CN_x) species on the SiO_2-surface at mild temperature, which further slowly acted to release active nitrogen species for controlled nitridation. The electronic properties of Ta were tuned by the different nitridation levels in TaON and Ta_3N_5 NPs. This controlled nitridation significantly improved the activity for alkene epoxidation, as compared to Ta_2O_5 NPs.

Two-dimensional carbon materials ranging from free-standing monolayers to oligo-layered graphenes could be obtained by the calcination of glucose in the presence of *in situ* generated layered graphitic carbon nitride using dicyandiamide as a sacrificial "soft" template, as reported by Li and Antonietti (Fig. 12).[19] The simple synthetic process required neither catalyst nor solvent and was used to convert glucose directly into polycrystalline carbon sheets having a "patched" multidomain graphene structure with lateral domains 2–15 nm in size. The obtained carbon assemblies exhibit high conductivity, high specific surface area, and unexpectedly good solution processability. The authors also extended the synthesis strategy to incorporate boron and nitrogen into the graphene network, thus creating excellently selective catalysts for organic oxidation reactions.[88]
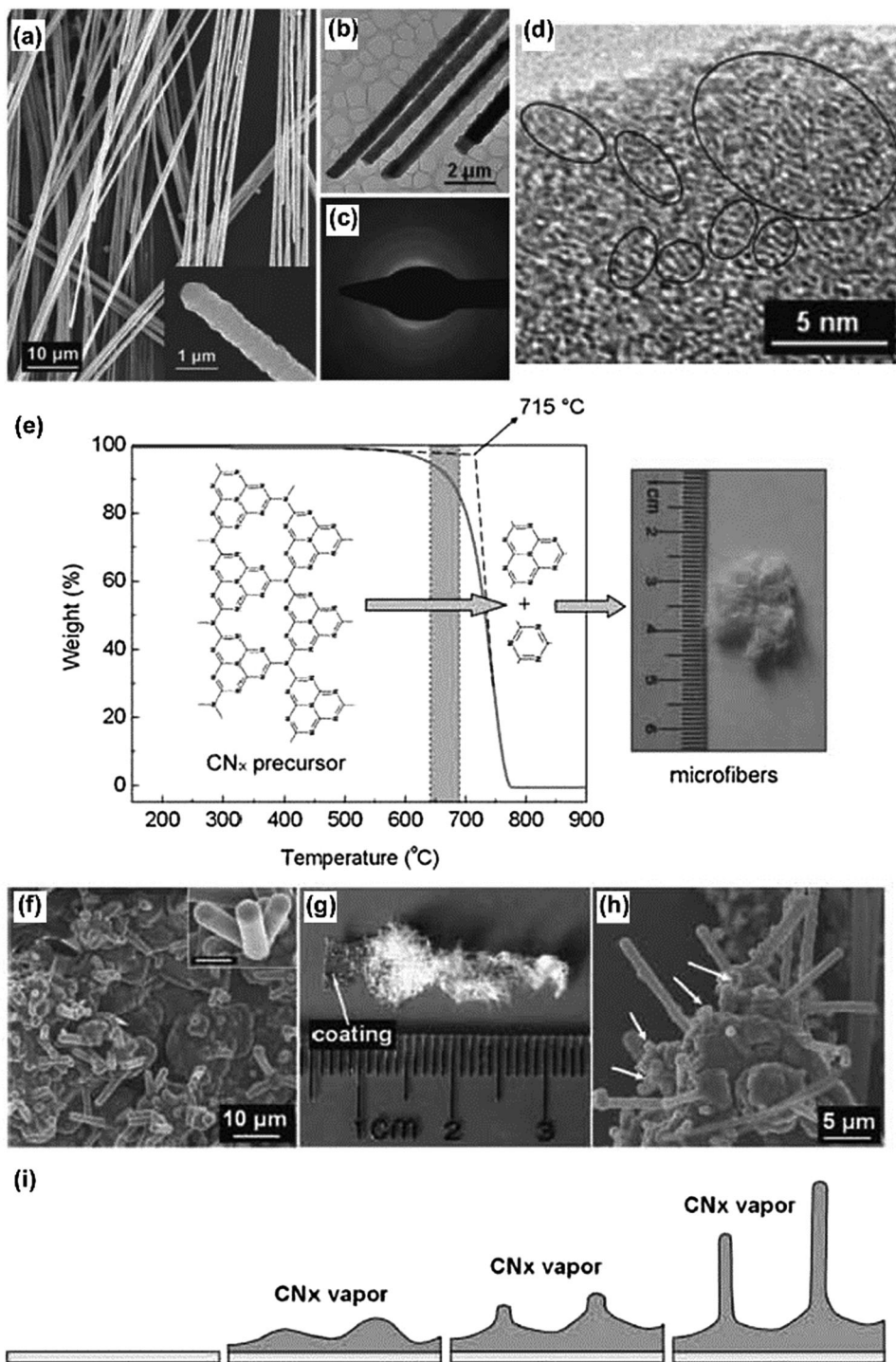
Fig. 11 (a) A SEM image of the as-obtained carbon nitride microfibers. The inset shows the tip of an isolated microfiber. (b) TEM image of carbon nitride microfibers, and (c) corresponding selected area electron diffraction (SAED) pattern. (d) High-resolution TEM image of a carbon nitride microfiber, revealing that the product has graphitic structure. (e) Thermogravimetric analysis result for the carbon nitride precursor and schematic illustration of carbon nitride microfiber formation. (f–i) The schematic process of the vapor–solid governed growth of carbon nitride microfibers by investigating the substrate. (Reproduced with permission from ref. 40. Copyright (2008) the Wiley-VCH.)

5. Summary and outlook

Only less than 10 years ago, an essentially neglected material, graphitic carbon nitride, was revived to a new level as a heterogeneous organocatalyst and was found to be a photocatalyst to produce hydrogen under visible light. This already stimulated broader research on pursuing pathways for an affordable, clean energy future based on this material and its derivatives.
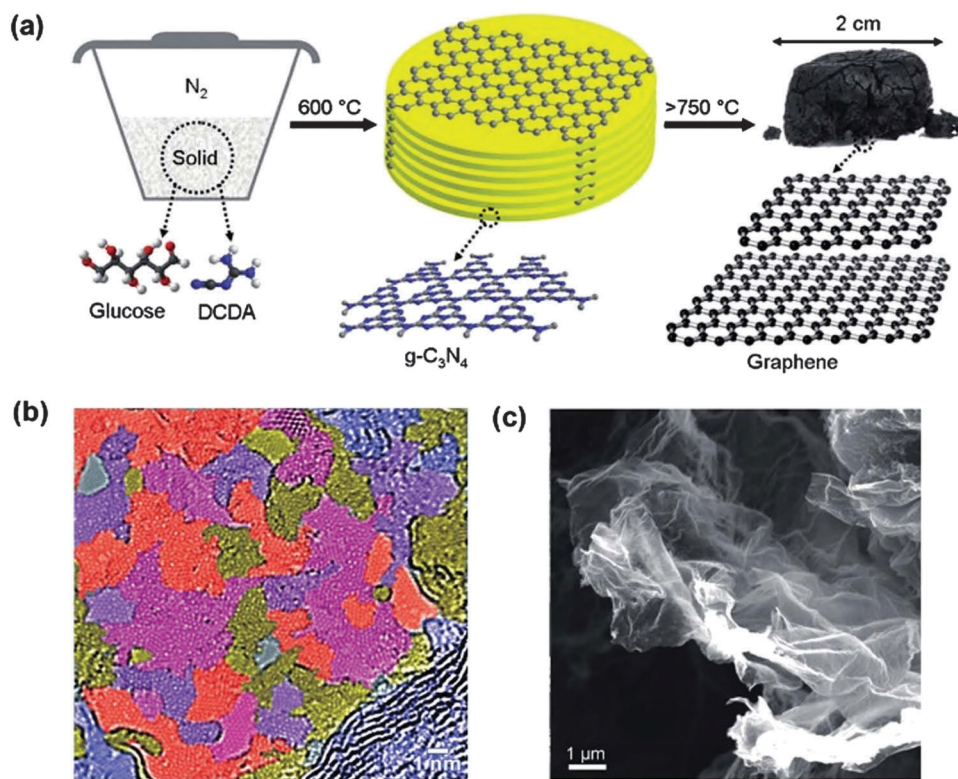
Fig. 12 (a) Proposed synthetic protocol for free-standing graphene. Bottom: Repetition motifs of an ideal g-C$_3$N$_4$ plane and of graphene. (b) SEM images of the as-formed graphene sample with high magnification. (c) High-resolution TEM image of the graphene-like structure of the graphene sheet. (Reproduced with permission from ref. 19. Copyright (2012) the Wiley-VCH.)

Its unique electronic structure with both an appropriate bandgap and band position to run relevant oxidation and reduction processes, as well as its high stability against temperature, acids, bases, and organic solvents, are intrinsic features favorable for applications also beyond photocatalysis. As this comes with facile synthesis, low price, non-toxicity, metal-free character, and photoelectric effects, it is *a posteriori* no surprise that g-C$_3$N$_4$ related research has meanwhile spread out to an even much broader range of applications that are beyond conventional catalysis scopes, far beyond what we could imagine in its starting. The current review is aiming to illustrate in a timely manner the versatility and importance of g-C$_3$N$_4$ in these new applications, where of course the transition from the already well-reviewed "older" applications is fluent. These applications include novel ultra-sensitive sensing, stable and photobleaching-poor bioimaging, drug delivery, novel photovoltaic and light emitting devices, data storage, but also processes like templating of novel materials and device manufacturing, including remnant molecular data storage.

Based on these findings and the newly disclosed properties, we believe that the exploration of potential g-C$_3$N$_4$ application just has started. This is also to say that this review, although detailed, can hardly cover all aspects even of the selected novel topics. Nevertheless, the research outlined here should be suitable to some extent convince the readers that g-C$_3$N$_4$ is not an old fashion but is continuing to bring more exciting chemistry with a wide range of applications.

Though many emerging applications are summarized in the above sections, there are still a bunch of studies located outside where we dare to list them as perspectives of the field. (i) For instance, ultrathin g-C$_3$N$_4$ nanosheets with hydrogen dangling bonds can be regarded as new metal-free room temperature ferromagnetic two dimensional nanomaterials. The introduced hydrogen dangling bonds into the g-C$_3$N$_4$ nanosheets can induce intrinsic ferromagnetism, and the saturation magnetization value of the g-C$_3$N$_4$ ultrathin nanosheets at room temperature was as high as 0.015 emu g^{-1}.[89] By employing first-principles calculations based on density functional theory, Li *et al.* showed that nonmagnetic g-C$_3$N$_4$ patterned in the form of a kagome lattice becomes ferromagnetic with its magnetic properties further enhanced by applying external strain.[90] We assume that more of these promising properties can be explored by the synergy of the unique covalent structure and the special π-conjugated aromaticity of the material.

(ii) For the use in structural hybrids, Shi *et al.* showed that the integration of g-C$_3$N$_4$ nanosheets into a polymer with interfacial hydrogen bonding interactions between the two could greatly improve the thermal stability and the mechanical properties of the polymer.[91] Specifically, with the addition of 6.0 wt% g-C$_3$N$_4$, the tensile strength of sodium alginate nanocomposite films was dramatically enhanced by 103%, while the Young's modulus remarkably increased from 60 to 3540 MPa. In particular, in the area of aqueous hydrogels partly touched also in the main text, we expect to see a number of new hybrid systems based on the principle. Here, we also want to mention

that such hybrids for instance enable a highly improved resolution in gel-electrophoresis,[92] an effect we attribute to local field effects within such dielectric structure media.

(iii) Combined with reduced graphene oxide, g-C_3N_4/rGO was proven by Wang *et al.* to be an effective modifier for porous polyethersulfone substrates in forming a thin film composite to set-up osmosis membranes.[93] The very efficient water permeability in such a modified membrane could be mainly attributed to the optimization of pore structures and improved wettability; (iv) Oh *et al.* reported the regenerative and selective CO_2 capture by metal-free large surface area carbon nitride heterostructures (Fig. 13).[94] It was analyzed that the strong dipole interaction induced by electron-rich nitrogen at nonplanar microporous carbon nitride geometry enforces the specific and reversible adsorption of CO_2 under ambient conditions. The resultant composite structure exhibited a CO_2 adsorption capacity under ambient conditions (0.43 mmol g^{-1}) and high CO_2 selectivity against N_2. The authors employed first-principles thermodynamics calculations to reveal that the microporous edges of graphitic carbon nitride offer the optimal CO_2 adsorption by induced dipole interaction and allow excellent CO_2 selectivity as well as facile regeneration ability. We expect that this is just the tip of a much broader research area to come, as the chemoselectivity of carbon nitride interactions also for other gases by far exceeds the one of the corresponding carbons and silica and can in addition be tuned by metal doping, as described in the sensing chapters.

(v) Exfoliated g-C_3N_4 nanosheets could form a stable sol in the aqueous solution. Under some extreme conditions, Zhang and coworkers reported that g-C_3N_4 could be dissolved and form true thermodynamic solutions in concentrated sulfuric acid, with g-C_3N_4 concentration up to 300 mg mL^{-1} ($\sim$14 wt%) at room temperature.[50] Due to the 2000 time higher concentration than those of previous dispersions, the first successful liquid-state NMR spectra of g-C_3N_4 were obtained, and a lyotropic liquid crystal phase of g-C_3N_4 was also observed. It is believed that such and similar solubilization methods and the alignment in a liquid crystalline state will open a new era of g-C_3N_4 processing for broader applications.

Actually, the more we try to understand about this material, the more unexpected chemistry and physicochemical properties are discovered, and more room can be accessed for picturing its colorful future. As the g-C_3N_4 renaissance research is going to enter the second decade, however, the past research and achievements also left us many questions to answer, which were categorized into three main aspects herein. First of all, predictable and controllable methods to synthesize nanostructured g-C_3N_4 particles, nanosheets, aggregates, and films remain an active target, as there is much to control and improve. Theoretical understanding of the structure formation and evolution should join these efforts to direct the experimental synthesis. Second, engineering aspects such as device development toward practical applications should be more emphasized, including
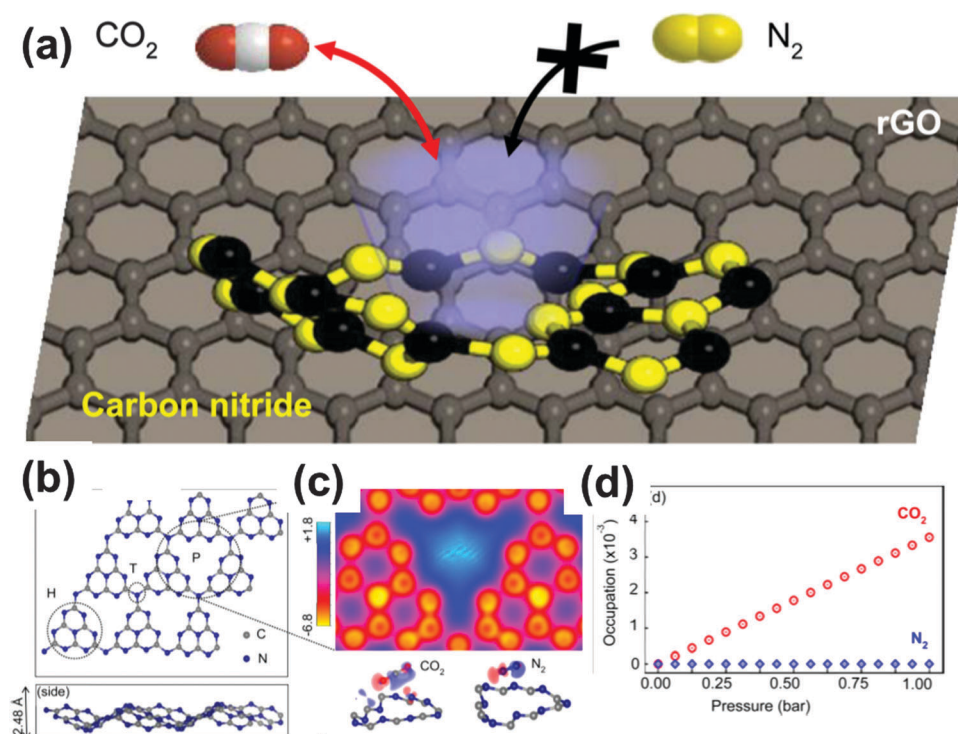

Fig. 13 (a) Schematic illustration of carbon nitride aerogel for selective CO_2 gas capture against N_2. (b) Density function theory (DFT) analysis of gas adsorption. Optimized geometry of heptazine-based g-C_3N_4 (top and side view, respectively). (c) Averaged DFT adsorption energies of single CO_2/N_2 at the pore site (P), heptazine (H) and tertiary N (T), in comparison with pristine graphene. (d) Estimated CO_2/N_2 occupation number as a function of the total pressure (10% CO_2 and 90% N_2), following first-principles thermodynamics and grand canonical ensemble formalism. (Adapted with permission from ref. 94. Copyright (2015) American Chemical Society.)

2324 | *Chem. Soc. Rev.*, 2016, **45**, 2308–2326

This journal is © The Royal Society of Chemistry 2016

photoelectrodes, environmental low price sensors, bioimaging, solar cells, *etc.* Therein, the performance of the g-C$_3$N$_4$ based devices is centrally based on the material composition and structures. With an optimized material composition and structure, for instance the solar energy conversion efficiency can certainly be further enhanced, or the response speed and detection capacity of sensors could also be improved. Such improvements are however only possible in close cooperation with physicists and engineers. Last but not the least, a deep and comprehensive understanding of the g-C$_3$N$_4$ based electronic structure, also in the excited states, should be pursued. Fundamental *ab initio* theoretical studies as well as molecular simulations are highly desirable to understand the underlying phenomena to guide the improvement in a model-based sense.

With that and all the very promising examples of the new effects of only the last 2–3 years in mind, we have good reasons to believe that the g-C$_3$N$_4$ based work remains a hotspot of modern materials chemistry, and we firmly believe the efforts devoted to its study will likely pay off for society in a very near future.

Acknowledgements

References

1 J. V. Liebig, *Ann. Pharm.*, 1834, **10**, 10.
2 L. Gmelin, *Ann. Pharm.*, 1835, **15**, 252.
3 A. Y. Liu and M. L. Cohen, *Science*, 1989, **245**, 841–842.
4 F. Goettmann, A. Fischer, M. Antonietti and A. Thomas, *Angew. Chem., Int. Ed.*, 2006, **45**, 4467–4471.
5 X. Wang, K. Maeda, A. Thomas, K. Takanabe, G. Xin, J. M. Carlsson, K. Domen and M. Antonietti, *Nat. Mater.*, 2009, **8**, 76–80.
6 Q. Han, B. Wang, Y. Zhao, C. Hu and L. Qu, *Angew. Chem., Int. Ed.*, 2015, **54**, 11433.
7 J. Sun, J. Zhang, M. Zhang, M. Antonietti, X. Fu and X. Wang, *Nat. Commun.*, 2012, 1139.
8 J. Liu, Y. Liu, N. Liu, Y. Han, X. Zhang, H. Huang, Y. Lifshitz, S.-T. Lee, J. Zhong and Z. Kang, *Science*, 2015, **347**, 970–974.
9 Y. Zheng, Y. Jiao, Y. Zhu, L. H. Li, Y. Han, Y. Chen, A. Du, M. Jaroniec and S. Z. Qiao, *Nat. Commun.*, 2014, **5**, 3783.
10 M. Shalom, S. Gimenez, F. Schipper, I. Herraiz-Cardona, J. Bisquert and M. Antonietti, *Angew. Chem.*, 2014, **126**, 3728–3732.
11 J. Liang, Y. Zheng, J. Chen, J. Liu, D. Hulicova-Jurcakova, M. Jaroniec and S. Z. Qiao, *Angew. Chem., Int. Ed.*, 2012, **51**, 3892–3896.
12 E. Z. Lee, Y. S. Jun, W. H. Hong, A. Thomas and M. M. Jin, *Angew. Chem., Int. Ed.*, 2010, **49**, 9706–9710.
13 J. Tian, Q. Liu, A. M. Asiri, A. O. Al-Youbi and X. Sun, *Anal. Chem.*, 2013, **85**, 5595–5599.
14 Q. Wang, W. Wang, J. Lei, N. Xu, F. Gao and H. Ju, *Anal. Chem.*, 2013, **85**, 12182–12188.
15 X. Zhang, H. Wang, H. Wang, Q. Zhang, J. Xie, Y. Tian, J. Wang and Y. Xie, *Adv. Mater.*, 2014, **26**, 4438–4443.
16 C. Cheng, Y. Huang, X. Tian, B. Zheng, Y. Li, H. Yuan, D. Xiao, S. Xie and M. M. Choi, *Anal. Chem.*, 2012, **84**, 4754–4759.
17 X. Zhang, X. Xie, H. Wang, J. Zhang, B. Pan and Y. Xie, *J. Am. Chem. Soc.*, 2012, **135**, 18–21.
18 J. Xu, T. J. Brenner, L. Chabanne, D. Neher, M. Antonietti and M. Shalom, *J. Am. Chem. Soc.*, 2014, **136**, 13486–13489.
19 X. H. Li, S. Kurasch, U. Kaiser and M. Antonietti, *Angew. Chem., Int. Ed.*, 2012, **51**, 9689–9692.
20 F. Zhao, H. Cheng, Y. Hu, L. Song, Z. Zhang, L. Jiang and L. Qu, *Sci. Rep.*, 2014, **4**, 5882.
21 Y. Wang, X. Wang and M. Antonietti, *Angew. Chem., Int. Ed.*, 2012, **51**, 68–89.
22 S. Cao, J. Low, J. Yu and M. Jaroniec, *Adv. Mater.*, 2015, **27**, 2150–2176.
23 A. Thomas, A. Fischer, F. Goettmann, M. Antonietti, J.-O. Müller, R. Schlögl and J. M. Carlsson, *J. Mater. Chem.*, 2008, **18**, 4893–4908.
24 Y. S. Jun, E. Z. Lee, X. Wang, W. H. Hong, G. D. Stucky and A. Thomas, *Adv. Funct. Mater.*, 2013, **23**, 3661–3667.
25 M. Shalom, S. Inal, C. Fettkenhauer, D. Neher and M. Antonietti, *J. Am. Chem. Soc.*, 2013, **135**, 7118–7121.
26 M. Groenewolt and M. Antonietti, *Adv. Mater.*, 2005, **17**, 1789–1792.
27 J. Huang, M. Antonietti and J. Liu, *J. Mater. Chem. A*, 2014, **2**, 7686–7693.
28 J. Zhang, M. Zhang, C. Yang and X. Wang, *Adv. Mater.*, 2014, **26**, 4121–4126.
29 S. Yang, Y. Gong, J. Zhang, L. Zhan, L. Ma, Z. Fang, R. Vajtai, X. Wang and P. M. Ajayan, *Adv. Mater.*, 2013, **25**, 2452–2456.
30 Y. Zhang, A. Thomas, M. Antonietti and X. Wang, *J. Am. Chem. Soc.*, 2008, **131**, 50–51.
31 P. Niu, L. Zhang, G. Liu and H. M. Cheng, *Adv. Funct. Mater.*, 2012, **22**, 4763–4770.
32 K. Schwinghammer, M. B. Mesch, V. Duppel, C. Ziegler, J. r. Senker and B. V. Lotsch, *J. Am. Chem. Soc.*, 2014, **136**, 1730–1733.
33 G. Algara-Siller, N. Severin, S. Y. Chong, T. Björkman, R. G. Palgrave, A. Laybourn, M. Antonietti, Y. Z. Khimyak, A. V. Krasheninnikov and J. P. Rabe, *Angew. Chem., Int. Ed.*, 2014, **53**, 7450–7455.
34 J. Liu, H. Wang, Z. P. Chen, H. Moehwald, S. Fiechter, R. van de Krol, L. Wen, L. Jiang and M. Antonietti, *Adv. Mater.*, 2015, **27**, 712–718.
35 J. Bian, Q. Li, C. Huang, J. Li, Y. Guo, M. Zaw and R.-Q. Zhang, *Nano Energy*, 2015, **15**, 353–361.
36 L. Jia, H. Wang, D. Dhawale, C. Anand, M. A. Wahab, Q. Ji, K. Ariga and A. Vinu, *Chem. Commun.*, 2014, **50**, 5976–5979.
37 X.-H. Li, J. Zhang, X. Chen, A. Fischer, A. Thomas, M. Antonietti and X. Wang, *Chem. Mater.*, 2011, **23**, 4344–4348.
38 J. Liu, R. Cazelles, H. Zhou, A. Galarneau and M. Antonietti, *Phys. Chem. Chem. Phys.*, 2014, **16**, 14699–14705.
39 J. Liu, J. Huang, D. Dontsova and M. Antonietti, *RSC Adv.*, 2013, **3**, 22988–22993.

This journal is © The Royal Society of Chemistry 2016

Chem. Soc. Rev., 2016, **45**, 2308–2326 | 2325

View Article Online

Chem Soc Rev   Review Article

40 Y. Zhao, Z. Liu, W. Chu, L. Song, Z. Zhang, D. Yu, Y. Tian, S. Xie and L. Sun, *Adv. Mater.*, 2008, **20**, 1777–1781.

41 Q. Guo, Y. Xie, X. Wang, S. Zhang, T. Hou and S. Lv, *Chem. Commun.*, 2004, 26–27.

42 J. Li, C. Cao and H. Zhu, *Nanotechnology*, 2007, **18**, 115605.

43 S.-W. Bian, Z. Ma and W.-G. Song, *J. Phys. Chem. C*, 2009, **113**, 8668–8672.

44 S. Barman and M. Sadhukhan, *J. Mater. Chem.*, 2012, **22**, 21832–21837.

45 S. Zhang, J. Li, M. Zeng, J. Xu, X. Wang and W. Hu, *Nanoscale*, 2014, **6**, 4157–4162.

46 J. Zhou, Y. Yang and C.-y. Zhang, *Chem. Commun.*, 2013, **49**, 8605–8607.

47 J. Liu and M. Antonietti, *Energy Environ. Sci.*, 2013, **6**, 1486–1493.

48 Y. Zhang, Q. Pan, G. Chai, M. Liang, G. Dong, Q. Zhang and J. Qiu, *Sci. Rep.*, 2013, **3**, 1943.

49 C. Cheng, Y. Huang, J. Wang, B. Zheng, H. Yuan and D. Xiao, *Anal. Chem.*, 2013, **85**, 2601–2605.

50 Z. Zhou, J. Wang, J. Yu, Y. Shen, Y. Li, A. Liu, S. Liu and Y. Zhang, *J. Am. Chem. Soc.*, 2015, **137**, 2179–2182.

51 B. Zhu, P. Xia, W. Ho and J. Yu, *Appl. Surf. Sci.*, 2015, **344**, 188–195.

52 X. Bai, S. Yan, J. Wang, L. Wang, W. Jiang, S. Wu, C. Sun and Y. Zhu, *J. Mater. Chem. A*, 2014, **2**, 17521–17529.

53 E. Kroke, M. Schwarz, E. Horath-Bordon, P. Kroll, B. Noll and A. D. Norman, *New J. Chem.*, 2002, **26**, 508–512.

54 L. Basabe-Desmonts, D. N. Reinhoudt and M. Crego-Calama, *Chem. Soc. Rev.*, 2007, **36**, 993–1017.

55 J. Tian, Q. Liu, A. M. Asiri, A. H. Qusti, A. O. Al-Youbi and X. Sun, *Nanoscale*, 2013, **5**, 11604–11609.

56 T. Y. Ma, Y. Tang, S. Dai and S. Z. Qiao, *Small*, 2014, **10**, 2382–2389.

57 M. Rong, L. Lin, X. Song, Y. Wang, Y. Zhong, J. Yan, Y. Feng, X. Zeng and X. Chen, *Biosens. Bioelectron.*, 2015, **68**, 210–217.

58 X.-L. Zhang, C. Zheng, S.-S. Guo, J. Li, H.-H. Yang and G. Chen, *Anal. Chem.*, 2014, **86**, 3426–3434.

59 Y. Liu, Q. Wang, J. Lei, Q. Hao, W. Wang and H. Ju, *Talanta*, 2014, **122**, 130–134.

60 Y. Zhang, X. Bo, A. Nsabimana, C. Luhana, G. Wang, H. Wang, M. Li and L. Guo, *Biosens. Bioelectron.*, 2014, **53**, 250–256.

61 H. Xu, J. Yan, X. She, L. Xu, J. Xia, Y. Xu, Y. Song, L. Huang and H. Li, *Nanoscale*, 2014, **6**, 1406–1415.

62 W. Ma, D. Han, M. Zhou, H. Sun, L. Wang, X. Dong and L. Niu, *Chem. Sci.*, 2014, **5**, 3946–3951.

63 Z. Zhang, J. Huang, Q. Yuan and B. Dong, *Nanoscale*, 2014, **6**, 9250–9256.

64 A. Du, S. Sanvito, Z. Li, D. Wang, Y. Jiao, T. Liao, Q. Sun, Y. H. Ng, Z. Zhu and R. Amal, *J. Am. Chem. Soc.*, 2012, **134**, 4393–4397.

65 H. Zhang, Q. Huang, Y. Huang, F. Li, W. Zhang, C. Wei, J. Chen, P. Dai, L. Huang and Z. Huang, *Electrochim. Acta*, 2014, **142**, 125–131.

66 J. K. Wassei and R. B. Kaner, *Acc. Chem. Res.*, 2013, **46**, 2244–2253.

67 L.-S. Lin, Z.-X. Cong, J. Li, K.-M. Ke, S.-S. Guo, H.-H. Yang and G.-N. Chen, *J. Mater. Chem. B*, 2014, **2**, 1031–1037.

68 Y. Tang, H. Song, Y. Su and Y. Lv, *Anal. Chem.*, 2013, **85**, 11876–11884.

69 Y. Sui, J. Liu, Y. Zhang, X. Tian and W. Chen, *Nanoscale*, 2013, **5**, 9150–9155.

70 J. Liu, J. Huang, H. Zhou and M. Antonietti, *ACS Appl. Mater. Interfaces*, 2014, **6**, 8434–8440.

71 R. Cazelles, J. Liu and M. Antonietti, *ChemElectroChem*, 2015, **2**, 333–337.

72 Y. Shiraishi, S. Kanazawa, Y. Sugano, D. Tsukamoto, H. Sakamoto, S. Ichikawa and T. Hirai, *ACS Catal.*, 2014, **4**, 774–780.

73 Y. Shiraishi, Y. Kofuji, H. Sakamoto, S. Tanaka, S. Ichikawa and T. Hirai, *ACS Catal.*, 2015, **5**, 3058–3066.

74 B. Kiskan, J. Zhang, X. Wang, M. Antonietti and Y. Yagci, *ACS Macro Lett.*, 2012, **1**, 546–549.

75 M. Liu, Y. Ishida, Y. Ebina, T. Sasaki and T. Aida, *Nat. Commun.*, 2013, **4**, 2029.

76 M. Woźnica, N. Chaoui, S. Taabache and S. Blechert, *Chem. – Eur. J.*, 2014, **20**, 14624–14628.

77 K. Sunada, Y. Kikuchi, K. Hashimoto and A. Fujishima, *Environ. Sci. Technol.*, 1998, **32**, 726–728.

78 J. Huang, W. Ho and X. Wang, *Chem. Commun.*, 2014, **50**, 4338–4340.

79 W. Bing, Z. Chen, H. Sun, P. Shi, N. Gao, J. Ren and X. Qu, *Nano Res.*, 2014, **8**, 1648–1658.

80 M. Chhowalla, H. S. Shin, G. Eda, L.-J. Li, K. P. Loh and H. Zhang, *Nat. Chem.*, 2013, **5**, 263–275.

81 Y. Zhang and M. Antonietti, *Chem. – Asian J.*, 2010, **5**, 1307.

82 J. Zhang, M. Zhang, L. Lin and X. Wang, *Angew. Chem., Int. Ed.*, 2015, **54**, 6297–6301.

83 D. Miyajima, H. Arazoe, M. Kawamoto, K. Akaike, Y. Koizumi and T. Aida, WO2014098251 (A1), 2014.

84 J. Xu, M. Shalom, F. Piersimoni, M. Antonietti, D. Neher and T. J. Brenner, *Adv. Opt. Mater.*, 2015, **3**, 913–917.

85 A. Fischer, M. Antonietti and A. Thomas, *Adv. Mater.*, 2007, **19**, 264–267.

86 A. Fischer, J. O. Müller, M. Antonietti and A. Thomas, *ACS Nano*, 2008, **2**, 2489–2496.

87 Q. Gao, S. Wang, Y. Ma, Y. Tang, C. Giordano and M. Antonietti, *Angew. Chem., Int. Ed.*, 2012, **51**, 961–965.

88 X. H. Li and M. Antonietti, *Angew. Chem., Int. Ed.*, 2013, **52**, 4572–4576.

89 K. Xu, X. Li, P. Chen, D. Zhou, C. Wu, Y. Guo, L. Zhang, J. Zhao, X. Wu and Y. Xie, *Chem. Sci.*, 2014, **6**, 283–287.

90 X. Li, J. Zhou, Q. Wang, Y. Kawazoe and P. Jena, *J. Phys. Chem. Lett.*, 2012, **4**, 259–263.

91 Y. Shi, S. Jiang, K. Zhou, C. Bao, B. Yu, X. Qian, B. Wang, N. Hong, P. Wen and Z. Gui, *ACS Appl. Mater. Interfaces*, 2013, **6**, 429–437.

92 M. Zarei, H. Ahmadzadeh, E. K. Goharshadi and A. Farzaneh, *Anal. Chim. Acta*, 2015, **887**, 245–252.

93 Y. Wang, R. Ou, H. Wang and T. Xu, *J. Membr. Sci.*, 2015, **475**, 281–289.

94 Y. Oh, V.-D. Le, U. N. Maiti, J. O. Hwang, W. Park, J. Lim, K. E. Lee, Y.-S. Bae, Y.-H. Kim and S. O. Kim, *ACS Nano*, 2015, **9**, 9148–9157.